www.elsevier.com/locate/pss

Thermospheric Density Model Biases at the 23rd Sunspot Maximum

C. Pardini, K. Moe, L. Anselmo

PII: S0032-0633(12)00062-1
DOI: doi:10.1016/j.pss.2012.03.004
Reference: PSS3278

To appear in: *Planetary and Space Science*

Received date: 19 December 2011
Revised date: 1 February 2012
Accepted date: 4 March 2012

Cite this article as: C. Pardini, K. Moe and L. Anselmo, Thermospheric Density Model Biases at the 23rd Sunspot Maximum, *Planetary and Space Science,* doi:10.1016/j.pss.2012.03.004

Thermospheric Density Model Biases at the 23rd Sunspot Maximum

C. Pardini[a*], K. Moe[b] and L. Anselmo[c]

[a,c] *Space Flight Dynamics Laboratory, ISTI/CNR – Consiglio Nazionale delle Ricerche – Pisa, Italy*
[b] *Space Environment Technologies, Irvine, California, USA*

[a] *E-mail: carmen.pardini@isti.cnr.it*
[b] *E-mail: kmmoe@att.net*
[c] *E-mail: luciano.anselmo@isti.cnr.it*

[*] *Corresponding author. Tel.: +39-050-315-2987; Fax: +39-050-315-2040;*
Postal address: ISTI/CNR, Via G. Moruzzi 1, 56124, Pisa, Italy.

Abstract

Uncertainties in the neutral density estimation are the major source of aerodynamic drag errors and one of the main limiting factors in the accuracy of the orbit prediction and determination process at low altitudes. Massive efforts have been made over the years to constantly improve the existing operational density models, or to create even more precise and sophisticated tools. Special attention has also been paid to research more appropriate solar and geomagnetic indices. However, the operational models still suffer from weakness. Even if a number of studies have been carried out in the last few years to define the performance improvements, further critical assessments are necessary to evaluate and compare the models at different altitudes and solar activity conditions.

Taking advantage of the results of a previous study, an investigation of thermospheric density model biases during the last sunspot maximum (October 1999 – December 2002) was carried out by analyzing the semi-major axis decay of four satellites: Cosmos 2265, Cosmos 2332, SNOE and Clementine. Six thermospheric density models, widely used in spacecraft operations, were analyzed: JR-71, MSISE-90, NRLMSISE-00, GOST-2004, JB2006 and JB2008. During the time span considered, for each satellite and atmospheric density model, a fitted drag coefficient was solved for and then compared with the calculated physical drag coefficient. It was therefore possible to derive the average density biases of the thermospheric models during the maximum of the 23rd solar cycle.

Below 500 km, all the models overestimated the average atmospheric density by amounts varying between +7% and +20%. This was an inevitable consequence of constructing thermospheric models from density data obtained by assuming a fixed drag coefficient, independent of altitude. Because the uncertainty affecting the drag coefficient measurements was about 3% at both 200 km and 480 km of altitude, the calculated air density biases below 500 km were statistically significant. The minimum average biases were obtained with JB2008, NRLMSISE-00 and GOST-2004.

Above 500 km, where only one satellite was analyzed (at 630 km), and errors tend to increase with altitude, it cannot be asserted that the calculated biases are significant. Nevertheless, they are presented to show how the various models diverge at higher altitudes. Around 630 km, NRLMSISE-00 had a negligible average bias, while the other models underestimated (GOST-2004) or overestimated the average density, by amounts varying between 6% and 16%. However, in terms of semi-major axis root mean square residuals, JB2006 and JB2008 were the best in any case.

Below 500 km, the short-term behavior of the models was also investigated by fitting the semi-major axis decay over 30-day arcs. The resulting fitted drag coefficients displayed a significant variability, probably associated with mismodeled density variations, but JB2008, followed by JB2006, provided the smallest semi-major axis residuals and a reduced short-term

variability of the density bias at just a few frequencies, having been probably successful in removing a significant fraction of the mismodeling sources.

Keywords

Thermospheric density model; Drag coefficient; Satellite orbital decay; Average density biases; Sunspot maximum.

1. Introduction

The thermospheric models used in orbital operations were developed at a time when little was known about satellite drag coefficients (Cook, 1966, 1965; Harris and Priester, 1965; Izakov, 1965; Jacchia, 1964; Wolverton, 1963). Thermospheric densities in low Earth orbit varied by several orders of magnitude, while the drag coefficients were uncertain by about 50% (Wolverton, 1963). The designers of these models wisely assumed a constant drag coefficient, often 2.2. During subsequent decades, information about gas-surface interactions in space has slowly accumulated from measurements involving paddlewheel satellites (which provided absolute thermospheric densities), mass spectrometers, pressure gauges, accelerometers, and satellites of various shapes and orientations. These measurements have been reviewed by Moe et al. (1995) and by Moe and Moe (2011a). These studies have established that satellite surfaces in low-Earth orbit are contaminated by adsorbed atomic oxygen and its reaction products, causing energy accommodation coefficients to be high, and the angular distribution of reemitted particles to be nearly diffuse (Moe and Moe, 2011a). This kind of gas-surface interaction is best described by the mathematical analysis (Sentman, 1961) which relates the drag coefficient to the velocity of the impinging particles, their initial temperature, the temperature of the particles after collision (related to the energy accommodation coefficient), and the geometry of the spacecraft. Consequently, it is now possible to calculate realistic (physical) drag coefficients as a function of altitude and solar activity for satellites of simple shapes (Bowman et al., 2008a; Bowman and Moe, 2006; Koppenwallner, 2011; Moe and Moe, 2005; Moe et al., 1995; Pardini et al., 2010; Pilinski et al., 2010). The recent paper by Pilinski et al. (2010) has investigated the important question of how atmospheric composition affects accommodation and drag coefficients. These studies have shown that physical drag coefficients of satellites of many shapes increase as the altitude increases. That increase is related to the decrease in the number of molecules adsorbed on satellite surfaces as altitude increases. Figure 1 is an example of the dependence of drag coefficients on altitude at times of sunspot minimum (Moe and Moe, 2005). It was constructed from data measured by paddlewheel satellites near solar minimum.

Since physical drag coefficients increase with altitude, while the densities used in constructing thermospheric models were measured using drag coefficients assumed to be independent of altitude, operational models inevitably have an altitude bias. These biases were measured for many satellites by calculating the difference between the fitted and physical drag coefficients (Bowman and Moe, 2006; Chao et al., 1997; Pardini et al., 2010). The real atmosphere functions on pressure levels, rather than on altitude, so referring accommodation coefficients to height alone omits the important influence of atmospheric composition. Pilinski et al. (2010) have recently addressed this limitation by using the Langmuir adsorption isotherm to investigate the effect of atomic oxygen on the accommodation coefficients at various altitudes.

In a previous study (Pardini et al., 2010), satellite drag and energy accommodation coefficients at altitudes up to 630 km were measured during the sunspot maxima of solar cycles 22 and 23 (around the years 1990 and 2000). In the process, the bias in the Jacchia-Bowman 2006 density model (Bowman et al., 2008b), which had been measured by Bowman (Personal communication, 2009) was confirmed.

Here, the previous work is extended to determine the bias in several other important operational thermospheric models. Knowledge of these model biases will facilitate the use of the models to calculate absolute densities, improve orbital predictions, and validate the ultraviolet spectrometric sensors, SSUSI (Special Sensor Ultraviolet Spectrographic Imager) and SSULI (Special Sensor Ultraviolet Limb Imager) on the Defense Meteorological Satellite Program (DMSP) satellites, and GUVI (Global Ultraviolet Imager) on the Thermosphere Ionosphere and Mesosphere Energy and Dynamics (TIMED) satellite (Emmert et al., 2006; Marcos, 2006a; Paxton et al., 1992).

After a review of some past and recent atmospheric density models, as well as of their solar and geomagnetic indices, the main upgrades and characteristics of the software tools and models used are introduced, together with the methodology adopted and the assumptions made to assess the density model biases, presented and discussed in the second part of this paper.

2. Modeling air drag on low Earth orbiting satellites

Aerodynamic drag is the largest non-gravitational perturbation acting on satellites in low-Earth orbit. The drag force, which is directed opposite to the satellite's velocity relative to the atmospheric flux, reduces the orbital energy and leads to a gradual decrease of the satellite's semi-major axis. Knowing the effects of air drag on the motion of satellites is of crucial importance for space operations, including trajectory determination, prediction and optimization, collision avoidance warnings, lifetime estimates, re-entry predictions, and orbital debris monitoring.

In aerodynamics, it is customary to express the drag force ($\boldsymbol{F}_D$) in the form:

$$\boldsymbol{F}_D = M\,\boldsymbol{a} = -\,1/2\;\rho\, C_D A\, V_r^2\, \boldsymbol{V}_r/V_r\ , \tag{1}$$

in which $\boldsymbol{a}$ is the corresponding acceleration, M is the mass of the satellite, ρ is the atmospheric density, $\boldsymbol{V}_r$ is the velocity of the satellite relative to the atmosphere, A is a reference area, frequently chosen as the cross-sectional area of the satellite facing the airstream, and C_D is the drag coefficient. The values of the area and the mass are often known within 1% (Moe et al., 2004), but the relative velocity, which depends on the complex dynamics of the Earth's atmosphere, may be affected by larger uncertainties. However, a reasonable approximation of $\boldsymbol{V}_r$ is obtained with the assumption that the atmosphere co-rotates with the Earth:

$$\boldsymbol{V}_r = \boldsymbol{V} - \boldsymbol{\omega}_\oplus \times \boldsymbol{r}\ , \tag{2}$$

where $\boldsymbol{V}$ is the satellite inertial velocity, $\boldsymbol{r}$ is the position vector, and $\boldsymbol{\omega}_\oplus$ is the Earth's angular velocity vector. Under most circumstances this assumption causes negligible errors. However, during major geomagnetic storms, atmospheric winds increase greatly. In such situations, it is possible to correct for the effects of in-track winds if the satellite carries two instruments which interact differently with the airstream (Moe et al., 2004). In general, the drag coefficient and the atmospheric density represent the principal causes of uncertainty in determining the drag force.

Therefore, if $\boldsymbol{F}_D$ is measured by satellite-borne accelerometers or by the observed orbital decay, it is the product $\rho\, C_D$ which is determined: any uncertainty in C_D produces an uncertainty in the air density ρ, and vice versa. Hence, due to mismodeled drag coefficients, the average atmospheric density might be affected by significant errors. In addition, other sources of uncertainty exist, including energy coming up from the lower atmosphere (Qian et al., 2009), inadequately modeled eddy diffusion removing energy from the thermosphere into the mesosphere, and inadequate solar and geomagnetic proxies used to model upper atmospheric heating (Moe and Moe, 2011b). Therefore, the uncertainties in the neutral density and its variations are the major sources of aerodynamic drag errors, and also the main limiting factor in the orbit determination and prediction process. Operational thermospheric models do have problems caused by thermospheric winds,

particularly during geomagnetic storms, and by the persistent inter-hemispheric exchange of species: Operational thermospheric models are not suited to treat these problems. General circulation models (Fuller-Rowell and Rees, 1980; Fuller-Rowell et al., 1994) are better suited for those purposes, although they often are too slow for operational applications. But it surely is true that the biases studied here do not apply during the major geomagnetic storms, which occur about 5% of the time. The thermospheric models themselves are in trouble at those times.

In recent years, a new modeling difficulty has arisen: thermospheric models have failed to predict the large density decrease at the 2008 solar minimum (Emmert et al., 2010). Although there has been a slow density decrease caused by increasing atmospheric carbon dioxide, this effect has been too small to explain the 2008 density decrease (Marcos et al., 2005; Solomon et al., 2010). Solomon, et al. think that most of the density decrease can be attributed to record low solar ultraviolet emission, while Moe and Moe (2011b) think that the decrease in the energy coming from the solar wind and magnetosphere is an important part of the problem. Bowman and Moe (2006) already showed that the density model biases vary with altitude, and differ at sunspot maximum and minimum. As the thermosphere changes, the biases will change. The biases measured during geomagnetically quiet and moderately disturbed times do not apply during the large geomagnetic storms that occur roughly 5% of the time, when the thermospheric circulation pattern is suddenly reversed, winds increase, and species are redistributed because of the enormous increase in energy deposited at high latitudes. At those times, tracking agencies often lose many satellites, and are more concerned to recover their lost satellites than to calculate model biases. In spite of these limitations, operational thermospheric models are used by many organizations. The models and their biases are relevant the other 95% of the time.

3. A review of some past and recent atmospheric density models

In spite of constant improvements, the atmospheric models still suffer from weakness. Even recent models have errors of about 10-15% under quiescent conditions, which grow to 30-60% at highly disturbed conditions (Volkov et al., 2008; Yurasov et al., 2004). The situation has not significantly changed over the last four decades. However, considerable efforts have been carried out to constantly improve the performances of the models, also thanks to new data sets from orbital decay, satellite-borne accelerometers and mass spectrometers, remote sensors, incoherent radar scattering, interferometers and so on, covering more than a solar activity cycle.

A number of different models have been published since the 1960's. The Jacchia models, developed between 1964 and 1977, were mainly based on satellite drag data. Their development used least squares solutions and a satellite drag coefficient of 2.2 below 300 km (Vallado and Finkleman, 2008). The Jacchia-Roberts 1971 (JR-71) model, which was originally derived from Jacchia 1970 (J70) and later on modified according to Jacchia 1971 (J71), was based on analytical solutions of the barometric and diffusion differential equations. JR-71 was also used by the Goddard Trajectory Determination System (GTDS) multipurpose computer code (Cappellari et al., 1976). Instead, the J71 model was adopted by the Committee on Space Research (COSPAR) as the International Reference Atmosphere 1972 (CIRA 1972).

The Mass Spectrometer and Incoherent Scatter (MSIS) models, developed between 1977 and 2002, utilized atmospheric composition data from satellites and temperatures from ground-based radars (Marcos, 2006b). The MSIS-86 version (Hedin, 1987) was adopted as the CIRA 1986 reference atmosphere at altitudes above 90 km. The Mass Spectrometer and Incoherent Scatter Radar Extended 1990 (MSISE-90) version (Hedin, 1991) describes the atmosphere from the ground level, while it is identical to MSIS-86 above 120 km. The more recent NRLMSISE-00 model (Picone et al., 2002) of the Naval Research Laboratory (NRL) extends from the ground to the exobase, and is a major upgrade of both the MSIS and Jacchia models. With its associated database, this model includes data on: (1) total mass density, from satellite accelerometers and orbit

determination (including the Jacchia data); (2) temperature, from incoherent scatter radars; (3) molecular oxygen (O_2) number density, from observations by the Solar Maximum Mission (SMM), based on solar ultraviolet occultation. The NRLMSISE-00 model is then able to describe the molecular composition of the Earth's atmosphere at different altitudes, as well as the overall density.

Another thermospheric density model, now mainly used by the French space agency (CNES) for orbitography purposes, is the Drag Temperature Model (DTM), firstly published by Barlier et al. in 1978. Originally based on total density measurements derived from satellite drag observations, it is continually upgraded by including new data from satellites, incoherent scatter radars and interferometers (Bruinsma et al., 2003). The latest version also includes density values from the CHAMP (Challenging Mini-satellite Payload) and GRACE (Gravity Recovery and Climate Experiment) accelerometers (Bruinsma and Forbes, 2007; Bruinsma et al., 2004).

The Thermospheric total Density model 1988 (TD-88) was derived mainly by fitting the density values from the DTM model with an analytical series of exponential functions in height and trigonometric functions in time (Sehnal, 1988; Sehnal and Pospisilova, 1988).

The empirical model GOST was constructed from observations of the orbital motion of the Russian Cosmos satellites. The atmospheric density was calculated using a simple analytical formula, whose factors represented the dependences on solar and geomagnetic activity, semi-annual effects and daily effects. The latest version of the model (GOST-2004) was issued by the State Committee on Standardization and Metrology of the Russian Federation (Volkov, 2004). It was based on artificial satellite drag data over the period 1964 to 2000.

Other models include the Marshall Space Flight Center (MSFC) Global Reference Atmosphere Model (GRAM) (Justus et al., 2004; see also see.msfc.nasa.gov/tte/model_gram.htm for the latest version, GRAM-2010) and the Marshall Engineering Thermosphere (MET) model (Owens, 2002). They were produced, on behalf of the National Aeronautics and Space Administration (NASA), to describe the terrestrial atmosphere from ground level upward for operational purposes, and were mainly based on the Jacchia models.

Recent improvements in the Jacchia models were made by Bowman and Tobiska (2006). The Jacchia-Bowman thermospheric density model 2006 (JB2006) was developed using the CIRA 1972 model (J71) as the basis for the diffusion equations. A new formulation of semi-annual density and exospheric temperature was employed (Bowman et al., 2008b), together with new solar irradiance indices (Tobiska et al., 2008). The more recent Jacchia-Bowman 2008 (JB2008) model was developed as an improved revision of the JB2006 model. New exospheric temperature and semi-annual density equations were developed, using additional solar indices derived from orbit-based sensor data. Geomagnetic storm effects were modeled using the disturbance storm time (Dst) index as the driver of global density changes. Also measurements from the CHAMP and GRACE accelerometers were used to validate the equations for geomagnetic storms (Bowman et al., 2008c).

In addition to the previous models, there are also techniques for improving or correcting the atmospheric densities. A first approach, consisting in adjusting a density model to agree with the average orbital decay of many satellites in real time, was pioneered in Russia by Andrey Nazarenko in the early 1980's and is known as Dynamic Calibration Atmosphere (DCA) (Bowman et al., 2005; Cefola et al., 2000; Doornbos et al., 2005; Marcos et al., 2000; Nazarenko and Yurasov, 2003; Nazarenko, 1999; Volkov and Yastrebov, 1990; Yurasov et al., 2006). Also the US Air Force High Accuracy Satellite Drag Model (HASDM) applied the DCA technique for density corrections of a revised version of the Jacchia 1970 model (Storz et al., 2002). However, the DCA techniques present several disadvantages (McLaughlin et al., 2011), including the limited spatial and temporal resolution of the corrections applied. A second method was suggested by the Naval Research Laboratory, and consists in using spectroscopic observations, acquired by ultraviolet spectrometers on DMSP satellites, to monitor the air density (Emmert, et al., 2006; Marcos, 2006a; Moe, 2006; Paxton, et al., 1992).

Many improvements in modeling the terrestrial air density have been made since the publication of the last series of CIRA models in 1986 (CIRA 1986). Therefore, the preparation of a new international reference atmosphere, CIRA 2008, has been endorsed at the COSPAR Assembly, in July 2008. CIRA 2008, which is currently in preparation, will recommend the models JB2008 and GRAM 2007 to compute the total mass density above 120 km, and the model NRLMSISE-00 to describe the structure and composition of the atmosphere from ground level upward.

3.1. Solar and geomagnetic inputs to the models

The sources of density variations in the thermosphere are primarily the solar extreme ultraviolet and soft X-ray fluxes (EUV and XUV), particle precipitation and electric fields. Changes in the EUV flux over a solar cycle give rise to significant variations of neutral temperature and density, causing changes, even by a factor of ten, in the drag acting on low Earth orbiting satellites.

Because the Earth's atmosphere does not allow the transmission of the extreme ultraviolet radiation, the solar radio flux at 2800 MHz (10.7 cm wavelength), $F_{10.7}$, which since the 1960's has been found to be fairly well correlated with the EUV radiation, has been used for many years as the primary proxy for it by most atmospheric models (Jacchia and MSIS series, TD-88, DTM, GRAM, MET, GOST, JB2006/2008). $F_{10.7}$ is expressed in solar flux units (sfu), where 1 sfu = 1×10^{-22} W m^{-2} Hz^{-1}, and is regularly observed on a daily basis from 1947.

In the past few years, new solar indices have been considered and employed by the Jacchia-Bowman and DTM models. The model JB2006 uses two other indices ($S_{10.7}$ and $M_{10.7}$) in addition to $F_{10.7}$ (Tobiska et al., 2008). Measurements of the index $S_{10.7}$, in the 26-34 nm solar EUV range, have been made since December 1995 with the Solar Extreme ultraviolet Monitor (SEM), on board the Solar and Heliospheric Observatory (SOHO). $S_{10.7}$ is expressed in solar flux units, as for $F_{10.7}$. The $M_{10.7}$ index is the core-to-wing ratio of the Mg II line at 280 nm reported in $F_{10.7}$ units (Heath and Schlesinger, 1986). The chromospheric Mg II line is operationally observed by the Solar Backscatter Ultraviolet (SBUV) spectrometer, originally hosted on board some of the National Oceanic and Atmospheric Administration (NOAA) operational satellites (e.g. NOAA 16, 17, 18).

In the JB2008 model, the new index $Y_{10.7}$ is used in addition to $F_{10.7}$, $S_{10.7}$ and $M_{10.7}$. It is a mixed solar index which is weighted to represent mostly the hot coronal 0.1-0.8 nm X-ray emission ($X_{10.7}$) during solar maximum and to represent mostly the chromospheric/transition region emission (Lyman-α at 121-122 nm) during moderate and low solar activity. The 0.1-0.8 nm X-ray emission is provided by the X-Ray Spectrometer (XRS) on the Geostationary Operational Environmental Satellites (GOES). Lyman-α has been observed by the SOLSTICE (Solar Stellar Irradiance Comparison Experiment) instrument on the Upper Atmosphere Research Satellite (UARS) and on the Solar Radiation and Climate Experiment (SORCE) satellite, and by the SEE (Solar Extreme ultraviolet Experiment) instrument on the TIMED satellite (Bowman et al., 2008c). Differently from $F_{10.7}$, many of the newer solar indices are available only back to 1997.

The French model DTM uses the Mg II index whenever possible to represent the solar EUV emission intensity instead of the flux $F_{10.7}$ (Bruinsma et al., 2004).

Besides the daily observed value of $F_{10.7}$ (together with $S_{10.7}$ and $M_{10.7}$ for JB2006; $S_{10.7}$, $M_{10.7}$ and $Y_{10.7}$ for JB2008), also the 81-day smoothed values are required in input by the atmospheric density models. These are: (1) the 81-day centered smoothed value of $F_{10.7}$ for the MSIS (e.g. MSISE-90 and NRLMSISE-00), the Jacchia (e.g. JR-71) and the Jacchia-Bowman series (e.g. JB2006 and JB2008); (2) the 81-day backward smoothed value of $F_{10.7}$ for GOST-2004; (3) the $S_{10.7}$ and $M_{10.7}$ 81-day centered smoothed values for JB2006 and JB2008; (4) the $Y_{10.7}$ 81-day centered smoothed value for JB2008.

The geomagnetic activity affects the air density through the delayed heating of the atmosphere, induced by charged energetic particles from the Sun. The most widely used geomagnetic planetary index, K_p, is a quasi-logarithmic worldwide average of the geomagnetic

activity recorded by twelve stations every three hours. The geomagnetic planetary amplitude, a_p, is a linear equivalent of the K_p index and eight values of a_p are averaged to create the daily planetary amplitude, A_p. Values of a_p range from 0 to 400, and are expressed in units of 2 nT. The scale of K_p is 0 to 9.

All density models use K_p or a_p (often the daily average A_p). In JB2008, the disturbance storm time (Dst) index is used in addition to A_p. The Dst index is determined from hourly measurements of the Earth's magnetic field from four off-equatorial observatories, and is reported in units of nT.

4. Performance assessment of the atmospheric density models at the 23rd sunspot maximum

A number of studies have been carried out in the last few years to characterize the performance improvements of some models relative to others (Akins et al., 2003; Marcos et al., 2000; Pardini and Anselmo, 2008a; Pardini and Anselmo, 2003; Pardini and Anselmo, 2001; Picone et al., 2001), to compare the computed density data with the observed data (Bezdek, 2007; Bowman et al., 2008a; Bruinsma and Forbes, 2007; Bruinsma et al., 2004; Doornbos et al., 2005; Emmert et al., 2006; McLaughlin et al., 2011; Moe and Moe, 2008; Volkov et al., 2008; Volkov and Suevalov, 2005), as well as to investigate the effects of various solar flux indices on the air density accuracy (Hongbo and Chagyin, 2009; Pardini et al., 2006). However, further accurate and critical assessments are necessary to evaluate and to compare density model performances at different altitudes and variable solar activity conditions.

In a previous study (Pardini et al., 2010), the energy accommodation coefficient and the physical drag coefficient were computed for a sample of satellites with altitudes between 200 and 630 km, during solar maximum conditions. Hence, taking advantage of these results, an investigation of thermospheric density model biases at the 23rd sunspot maximum was possible. The satellites reused for this analysis were: Cosmos 2265 and Cosmos 2332, both in elliptical orbit with average perigee altitude of about 275 km; SNOE (Student Nitric Oxide Explorer) and Clementine, in nearly circular orbit with mean perigee altitude around 480 km and 630 km, respectively. Their known physical characteristics (mass and cross-sectional area), along with the orbital elements at the beginning of the time span considered, are shown in Table 1. During the maximum of the last solar cycle 23 (from October 1999 to December 2002), biases were evaluated for the following density models: JR-71, MSISE-90, NRLMSISE-00, GOST-2004, JB2006 and JB2008.

4.1 Software tools and models

Two software codes, mainly developed by one of the authors (Pardini), were used for this study: CDFIT 5.0 and SATRAP 5.0. CDFIT, as made clear by its name, was specifically developed to fit the semi-major axis decay of low Earth satellites due to air drag by solving for the drag coefficient able to minimize the root mean square residuals between the propagated and observed semi-major axis, the latter obtained from the Two-Line Elements (TLE) sets (Hoots and Roehrich, 1980) available in the time span of interest. The Satellite Reentry Analysis Program (SATRAP) is an orbit propagator, originally developed for reentry predictions (Pardini and Anselmo, 1994), but actually applicable to all the circumterrestrial orbital regimes. Both software tools use the Cowell's method for the numerical integration of the equations of motion and an 8th order Runge-Kutta integration scheme with variable step-size control for propagation. The original architecture was based on the Artificial Satellite Analysis Program (ASAP), version 2.0 (Kwok, 1987), but many changes have been introduced over the years, in terms of input and output variables, Earth and force models, and Moon and Sun ephemerides.

CDFIT and SATRAP share the same common input parameters, physical constants, force models, propagation options, conversion routines and databases. The orbital perturbations considered are those due to geopotential zonal and tesseral harmonics, third body attraction of the Moon and the Sun, direct solar radiation pressure with eclipses, and aerodynamic drag. The default version of the geopotential model is EGM96 (Lemoine et al., 1998), but alternative coefficients can be selected, if needed. Concerning the ephemerides of the Moon and the Sun, two options are available: very fast analytic polynomial expansions disregarding the short-period variations of the luni-solar orbital elements, more than acceptable in most applications, or quite slower polynomial interpolations using the Chebyshev expansion coefficients of the high precision ephemeris files issued by the Jet Propulsion Laboratory (DE-405/DE-406). Regarding direct solar radiation pressure, an aspect area different from the cross-sectional area exposed to air drag can be provided in input, together with a radiation pressure coefficient, typically in the range from 1 to 2. The radiation pressure is computed taking into account the varying Sun-Earth distance and a simple geometrical representation of the sunlight shadowing due to the Earth (Kwok, 1987; Pardini and Anselmo, 2008b).

Over the years, special attention was paid to the implementation of various atmospheric density models for the representation of air drag. In version 5.0 of both CDFIT and SATRAP it is therefore possible to choose one of the following thermospheric models: United States Standard Atmosphere 1976 (Dubin et al., 1976), TD-88, JR-71, MSIS-86, MSISE-90, NRLMSISE-00, GOST-2004, JB2006 and JB2008. Moreover, for very low flying or reentering satellites, when the free molecular flow regime no longer applies, the drag coefficient is progressively adjusted as a function of the Knudsen number (Regan and Anandakrishnan, 1993).

4.2 Sources of thermospheric density models and solar-geomagnetic indices

All density models selected for this study had been implemented in CDFIT and SATRAP beginning from the literature and/or from the software codes available online.

The code for the JR-71 model was written in Fortran 77 using the documentation of the GDTS computer system (Cappellari et al., 1976). It uses the solar radio flux at 10.7 cm (with a lag of one day to account for the delay in the atmosphere response: i.e. the daily observed flux at the current epoch has to be that of the previous day) along with its 81-day centered smoothed value, as solar flux proxy, and the daily quasi-logarithmic geomagnetic index obtained from A_p to represent the geomagnetic activity.

The routines for GOST-2004 were written in Fortran 90 using the official documentation of the Russian standard model (Volkov, 2004), translated into English by Vasiliy S. Yurasov in 2006 and edited by Paul J. Cefola in 2007. The solar radiation proxy is the same as for JR-71, with differences in the lag of $F_{10.7}$ (1.7 days instead of 1 day) and in the 81-day average, which is not centered, but backward with respect to the current time. The input geomagnetic index is the daily A_p, delayed by 0.6 days.

The Fortran codes of the MSIS and Jacchia-Bowman models were instead available online. MSISE-90 and NRLMSISE-00 were provided by the US Naval Research Laboratory through their website on upper atmosphere (uap-www.nrl.navy.mil/uap). The input solar and geomagnetic indices were those of JR-71, with the same assumptions.

The Fortran sources of the Jacchia-Bowman models were provided by Space Environment Technologies (sol.spacenvironment.net/~JB2006/; sol.spacenvironment.net/~JB2008/). As previously pointed out, these models use new additional solar and geomagnetic indices with different lags: 1 day for $F_{10.7}$ and $S_{10.7}$ in both JB2006 and JB2008; 5 days for $M_{10.7}$ in JB2006 and 2 days for $M_{10.7}$ in JB2008; 5 days for $Y_{10.7}$ in JB2008. The input geomagnetic index is A_p for JB2006 and Dst for JB2008.

For the solar radio flux at 10.7 cm, the daily values measured at 20:00 UTC by the Dominion Radio Astrophysical Observatory (DRAO), in Penticton, British Columbia, were used. These are issued by the NOAA's National Geophysical Data Center (NGDC) in its website (ftp.ngdc.noaa.gov/STP/SOLAR_DATA/SOLAR_RADIO/FLUX/). For the time span considered in this study, corresponding to the sunspot maximum of cycle 23, the daily observed $F_{10.7}$ and its 81-day centered average are represented in Figure 2. Figure 3 shows, instead, the daily A_p, which is provided as well, along with the 3-hour K_p index, by NOAA/NGDC (ftp.ngdc.noaa.gov/STP/GEOMAGNETIC_DATA/INDICES/KP_AP/). Concerning the Jacchia-Bowman models, the historical values of the new solar and geomagnetic indices, which are available back to 1997, are those provided by Space Environment Technologies. Figure 4 represents the 81-day centered average of these solar radiation indices during the period of interest.

4.3 Drag coefficient estimation

With each density model (JR-71, MSISE-90, NRLMSISE-00, GOST-2004, JB2006 and JB2008), fitted drag coefficients (C_{DF}) were obtained, using CDFIT, for Cosmos 2265, Cosmos 2332 and SNOE over 1186 days (1 October 1999 – 30 December 2002), and for Clementine over 1123 days (4 December 1999 – 30 December 2002). During the time span considered, the observed mean semi-major axis decay was 354.1 km for Cosmos 2265, 287.5 km for Cosmos 2332, 129.1 km for SNOE and 32.6 km for Clementine. To propagate the trajectory, CDFIT took into account the following perturbations: geopotential harmonics (EGM96), up to the 16th order and degree; third body attraction of the Moon and the Sun (fast analytic polynomial expansions), direct solar radiation pressure with eclipses and, of course, aerodynamic drag.

The procedure adopted, for each satellite and atmospheric model, was the following. The mean semi-major axes corresponding to all TLEs available in the analyzed time interval were computed and considered as "pseudo-observations". TLEs were chosen simply because they were the sole reliable orbital elements freely available for the satellites analyzed in this study. No specific information concerning their intrinsic accuracy was accessible, but it is known that they are typically characterized by a position error of about 1 km (Vallado, 2007). This means that, even assuming that the whole position error derived from a bad estimation of the semi-major axis, which was the only orbit parameter used in the analysis, a corresponding typical inaccuracy of about 100 m was possible for the semi-major axis derived from each TLE.

However, such pseudo-observations were fitted, over short arcs of thirty days and long arcs of three years, using a high-precision special perturbations propagator and a conventional least-squares method. Each 30-day interval contained about 40-50 pseudo-observations (i.e. TLEs), so the contribution of the TLE errors to the semi-major axis root mean square residuals associated with the short arc fits were around 15 m. For the long arc fits, the corresponding figure was 2.5 m. These values were appropriately small with respect to the observed semi-major axis decay and the total residuals obtained with the short and long arc fits, making possible a meaningful comparison of the atmospheric models. (For Clementine, only the 3-year fit was carried out, just because the relatively moderate decay rate did not permit to clearly separate, over 30 days, the TLE inaccuracies from the other effects.)

Moreover, the specific experience with satellites of the type used in this study has shown that TLEs may be generally quite better in such cases, with position errors of 300-400 m (Vallado and Crawford, 2008) or mean motion, in revolutions per day, accurate to the sixth significant figure (King-Hele, 1987). Both estimates lead to TLE-derived semi-major axis errors around 30 m, corresponding to root mean square residuals of about 4.5 m over 30 days and < 1 m over 3 years.

Using the orbit predictor of CDFIT, and a preliminary guess of the drag coefficient, the trajectory was propagated in the chosen interval, using the first TLE, converted into osculating Cartesian elements (Hoots and Roehrich, 1980), as initial conditions. At each TLE epoch, the

difference between the propagated (a_{i_prop}) and the "observed" mean semi-major axis (a_{i_obs}) was computed and, at the end of the process, the related root mean square residuals (R) were obtained as follows:

$$R = \sqrt{\frac{\sum_{i=1}^{N}\left[a_{i\_obs} - a_{i\_prop}\right]^2}{N}} \quad , \tag{3}$$

in which i identifies the pseudo-observation and N is the total number of pseudo-observations available (i.e. the number of TLEs). Then, by varying a little bit the drag coefficient, the computation was repeated until the value of R was minimum. The corresponding value of the drag coefficient, which minimized the semi-major axis root mean square residuals of the propagation, was thus taken as the fitted drag coefficient (C_{DF}). The values so obtained are given in Table 2. The robustness of the drag coefficient fits was also checked against geopotential harmonics truncation (16 × 16 vs. 40 × 40), luni-solar perturbations (on/off) and solar radiation pressure (on/off). The maximum differences obtained in the worst cases were less than 0.5%.

SATRAP was instead used to propagate the initial TLEs up to the end of the time span of interest, by applying the fitted drag coefficients and the same perturbation models of CDFIT, in order to verify that the evolution of the propagated semi-major axis actually reproduced the observed decay.

Following the approach and the results outlined in Pardini et al. (2010), it was possible to estimate the physical drag coefficients (C_{DP}) of the four satellites, starting from the fitted drag coefficients (C_{DF}) – determined over the full time span – and from the known density biases of the JB2006 model (Bowman, Personal communication, 2009). In fact – taking into account that each satellite had known mass and cross-sectional area – the average density errors of JB2006, which were previously evaluated in comparable solar activity conditions, were used to properly rescale the values of C_{DF}, achieving a reasonable assessment of the actual, or physical, drag coefficients (Table 3).

5. Thermospheric model average density biases at the 23rd sunspot maximum

Having estimated the physical drag coefficients (C_{DP}) of the four satellites, the average density biases (in percent) of the thermospheric models were derived as:

$$100 \times \frac{C_{DP} - C_{DF}}{C_{DP}} \, . \tag{4}$$

Table 4 shows the biases computed for the selected density models. Here the sign "+" means that the atmospheric density is overestimated by the model, while the sign "–" means that the density is underestimated.

Below 500 km, all the models overestimated the atmospheric density. This was the inevitable consequence of constructing thermospheric models from data which assumed the drag coefficient to be independent of altitude. At the lowest mean altitude considered (275 km), the smallest average bias (+8%) was associated with the JB2008 model, followed by NRLMSISE-00 and GOST-2004 (+9%), MSISE-90 (+10%), JR-71 and JB2006 (+12%). As shown in Table 2, the best fit with the semi-major axis decay data, in terms of root mean square residuals, was obtained with JB2006 (1.0 km), followed by JB2008 (1.2 km), JR-71 (1.5 km), NRLMSISE-00 (1.8 km),

GOST-2004 (2.1 km) and MSISE-90 (2.3 km). Around 480 km, the smallest average bias (+7%) was associated with NRLMSISE-00 and GOST-2004, followed by JB2008 (+9%), MSISE-90 (+11%), JB2006 (+15%) and JR-71 (+20%). Regarding the semi-major axis root mean square residuals, the JB2008 and JB2006 models were the best (0.6-0.7 km), followed by GOST-2004 and JR-71 (0.9 km), MSISE-90 and NRLMSISE-00 (1.2 km).

Using data of Table 5 in Pardini et al. (2010), and the drag and accommodation coefficients tabulated in the Geophysical Monograph 87 (Moe et al., 1995), it was possible to calculate that the error in the drag coefficient of the satellites analyzed below 500 km was of the order of 3%, or less. Therefore, since the average model biases herein obtained were in between +7% and +20%, these biases are statistically significant.

On the other hand, above 500 km – where only one satellite was analyzed (at 630 km), and errors tend to increase with altitude – it cannot be asserted that the results are equally significant. Nevertheless, they are presented to show how the various models diverge at higher altitudes. In fact, around 630 km, GOST-2004 underestimated the atmospheric density (−11%), NRLMSISE-00 displayed a negligible bias, while all the other models continued to overestimate the average density by varying amounts: MSISE-90 by 6%, JB2008 by 9%, JB2006 by 15% and JR-71 by 16%. In terms of semi-major axis root mean square residuals, JB2008 and JB2006 again provided the best (0.2-0.3 km), followed by GOST-2004 and NRLMSISE-00 (0.4 km), MSISE-90 and JR-71 (0.5 km).

The large differences in the model biases at 630 km, presented in Table 4, were caused by the uncertainties in drag coefficients and in the biases of the thermospheric models as observed in earlier studies (Bowman and Moe, 2006; Chao et al, 1997; Moe, et al., 2004; Moe et al., 1998).

It is clear, from the semi-major axis root mean square residuals shown in Table 2, that all the models considered in the study are appropriate for most of the astrodynamics applications, because they are able to fit the observed orbital decay with comparable and relatively small residuals, taking into account the very long arc considered (more than 1100 days). The maximum difference among the models was, in fact, just about a factor of two. This is because even a significant constant density bias can be easily compensated by a properly rescaled drag coefficient (see Eq. 1), leaving the drag force unaffected. On the other hand, the semi-major axis root mean square residuals are the consequence of the mismodeling of orbit determinations and perturbations. As far as the drag modeling is concerned, the residuals are impacted by the ability of the models to match, as closely as possible, the density variations due to varying perigee altitude and argument, solar zenith angle, season, latitudinal excursion, solar and geomagnetic activity. Moreover, composition changes may affect the actual drag coefficient, contributing to the residuals as well.

Therefore, it should not be surprising to find that models affected by relatively higher average density biases, e.g. JB2006, may be characterized, at the same time, by comparatively lower residuals, while models with typically smaller average biases, e.g. NRLMSISE-00 and GOST-2004, may exhibit greater residuals. Overall, at least below 500 km, JB2008 presented the best combination in terms of smaller average density biases and semi-major axis root mean square residuals.

6. Short arc analysis

Trying to better characterize and compare the density models, fitted drag coefficients were also computed over 30-day arcs, covering the analyzed sunspot maximum time span. The analysis was carried out for the satellites below 500 km, i.e. Cosmos 2265, Cosmos 2332 and SNOE, where the effects of air drag on the semi-major axis were significant over the relatively short arcs. The results obtained with the various models are summarized in Figures 5-10, in terms of fitted drag coefficients obtained in each 30-day arc and of the corresponding semi-major axis root mean square residuals.

Of course, the C_{DF} obtained as a mean of the values found for each 30-day arc were not necessarily identical to those obtained by fitting the semi-major axis decay over the full time span analyzed. For Cosmos 2265, the mean of the short arc C_{DF} was lower by 2%, or less, with respect to the long arc value, with the exception of the GOST-2004 model, for which the mean was lower by approximately 3.5%. In the case of Cosmos 2332, on the other hand, the differences, positive or negative, were less than 1% for all the models. For SNOE, the mean of the short arc C_{DF} was

greater by 2%, or less, with respect to the long arc value, with the exception of the JR-71 model, for which the mean was higher by about 3.5%. These differences among mean short arc C_{DF} and long arc results may provide a guess of the consistency and accuracy of the model average density biases listed in Table 4.

Regarding the variability of the 30-day arc fitted drag coefficients around the mean values, it was minimum for JB2008, with a standard deviation (depending on the satellite) of 8-10%, followed by JB2006 (8-13%), NRLMSISE-00 (9-16%), MSISE-90 (10-16%), JR-71 (10-18%), and GOST-2004 (13-17%).

With reference to the semi-major axis root mean square residuals, Table 5 summarizes the mean values of the short arc fits and the corresponding standard deviations. The models provided comparable results, with average 30-day arc residuals of about 100 m for the two Cosmos satellites and approximately 70 m for SNOE. The ratio between the maximum and minimum mean values among the various models was 1.8 for Cosmos 2265, 1.4 for Cosmos 2332 and 1.2 for SNOE. The smallest residuals were consistently associated with JB2006 and JB2008, followed by NRLMSISE-00 and MSISE-90, JR-71 and GOST-2004. This order basically reflected that obtained on the basis of the dispersion of the 30-day arc fitted drag coefficients, suggesting that the observed variability was due, by a significant amount, to the mismodeling of atmospheric density.

In order to investigate the relative magnitude and possible origin of the fluctuations around the mean values discernible in Figures 5-10, concerning in particular the 30-day fitted drag coefficients and possibly linked to mismodeling effects, a Fourier analysis of the results obtained with each density model and satellite was carried out. The results are presented with the same scale in Figures 11-16, as periodograms based on the discrete fast Fourier transform applied to 38 thirty-day arcs, i.e. over 1140 days.

Of course, the interpretation of Figures 11-16 requires a particular caution. First of all, due to the arc length of 30 days, there is a Nyquist cutoff period two times as large, i.e. 60 days. Therefore, no signal with a period smaller than 60 days can be detected. At the same time, the maximum period identifiable has the identical duration of the finite time span considered, i.e. 1140 days. However, the number of unique period measurements in the Fourier transform is given by the number of arcs considered (38) divided by 2, i.e. 19. The corresponding periods are (in days): 60, 63.3, 67.1, 71.3, 76, 81.4, 87.7, 95, 103.6, 114, 126.7, 142.5, 162.9, 190, 228, 285, 380, 570, and 1140. Consequently, the period resolution is relatively good at low values, just above the Nyquist cutoff, but becomes significantly degraded above 4-5 months. This means, for example, that a signal with a yearly period cannot be easily and unambiguously identified in the plots.

That said, the periodograms obtained can anyway provide useful indications and insights on the observed fitted drag coefficient variability. First of all, it is clear that the observed drag coefficient variability is not random, but periodic, with most of the spectral power concentrated at certain periods. JB2008 seems quite successful in having removed a significant fraction of the time varying mismodeling sources (Figure 16). Concerning the Cosmos satellites, in elliptical orbits with low perigee, the only peaks left are probably linked to the precession of the perigee through the atmosphere, with a period of about 115 days in the inertial space, while for SNOE, in an orbit around 480 km, the main peak might perhaps be associated to a residual semi-annual effect and to the variation of the angle β between the orbit plane and the geocentric vector of the Sun. About the spectrum of the associated residuals, the fit adjustment of the drag coefficients over the 30-day arcs was able to remove any clear signature in the SNOE results, but for the Cosmos satellites some

unaccounted for effects clearly remained, with main peaks close to the perigee precession period and half of a year.

Regarding the JB2006 model, most of what has been said of JB2008 is still valid (Figure 15). For the Cosmos satellites, the periodogram of the fitted drag coefficients presents peaks only in correspondence of the perigee precession period, while for SNOE, in addition to a broad peak with about semi-annual periodicity, another sharp peak close to the perigee precession period (about 108 days) is present as well. With reference to the associated semi-major axis root mean square residuals, again no clear signature is present in the SNOE results, while only one semi-annual peak dominates the Cosmos 2265 plot. Lesser higher frequency terms, either linked to the perigee precession or of unknown origin, are also present, as in the case of JB2008.

The periodograms of MSISE-90 (Figure 12) and NRLMSISE-00 (Figure 13) are very similar. The drag coefficient spectrum of SNOE presents two significant peaks, with periods close to the perigee precession cycle and to one year. Regarding the other two satellites, no important peak is present in the Cosmos 2265 data, while a sharp and strong signal with a period close to that of the perigee precession is evident in the case of Cosmos 2332. The spectra of the residuals, on the other hand, do not show any clear connection with the drag coefficient plots and display peaks at several frequencies of no obvious meaning.

Coming to JR-71 (Figure 11), the drag coefficient periodogram of SNOE presents three prominent peaks: one close to the perigee precession period and the other two with approximately semi-annual and annual periodicities. The latter two might be possibly associated to mismodeled seasonal effects and to the evolution of the β angle. As far as the Cosmos satellites are concerned, no pronounced peak is present in the Cosmos 2265 data, while Cosmos 2332 displays a prominent peak with the period of the perigee precession and a quite lesser peak with semi-annual periodicity. Annual and semi-annual signals seem also present, with power depending on the satellite, in the periodogram of the semi-major axis residuals, but several other noticeable frequencies with no obvious explanation are evident as well. To be noticed, in particular, the strong signal with period of about 81 days (equivalent to three solar rotations), associated with Cosmos 2332. It is the main peak also in the MSISE-90 and NRLMSISE-00 residuals, and can be identified in the JB2006 and JB2008 plots as well.

Finally, with regard to GOST-2004 (Figure 14), the drag coefficient periodogram of SNOE presents again three prominent peaks: one close to the perigee precession period and the other two with approximately semi-annual and annual periodicities. As said in the previous cases, the latter two might possibly be associated with mismodeled seasonal effects and the evolution of the β angle. Moreover, all the five peaks present in the plot have the same periods of the five ones in the periodogram of JR-71, and of four out of six peaks present in the spectra of MSISE-90 and NRLMSISE-00. It should also be remarked that the two lowest power signals, appearing in the spectra of the latter two models with periods of 163 and 228 days, are replaced in JR-71 and GOST-2004 by a relatively stronger signal with the intermediate period of 190 days. Concerning the Cosmos satellites, the strongest component has a period of 76 days, without a corresponding term in all the other models. For Cosmos 2265, only one peak out of four, with a period of 104 days (not far from the duration of a full perigee precession), can be found also in the other models, with the partial exception of JB2008, in which the power reaches a maximum at 114 days. For Cosmos 2332, two peaks out of four, with periods of 95 and 114 days (again not far from the duration of a full perigee precession), can be found in the other models as well, apart from JB2008, in which only the 114-day component is present.

About the semi-major axis residuals of SNOE, the main component has a semi-annual periodicity and the overall frequency distribution is similar to those observed in the plots of the other models, again with the exception of JB2008, even though the relative amplitudes may vary from one model to the other. However, the spectra of the GOST-2004 residuals for the Cosmos satellites are quite different, in amplitude and frequency distributions, from those obtained with all the other thermospheric density models.

7. Conclusions

Taking advantage of the approach and the results of a previous study (Pardini et al., 2010), an investigation of thermospheric density model biases during the last sunspot maximum became possible. Including all the relevant orbital perturbations, six widely used atmospheric models were evaluated, as implemented in a recently upgraded software code used to fit the observed semi-major axis decay. The analysis made use of four satellites of known physical characteristics.

During the time span considered, for each satellite and atmospheric density model, a fitted drag coefficient was solved for, by applying the software to the observed semi-major axis decay, and then compared with the corresponding physical drag coefficient calculated as in the previous study. It was therefore possible to derive the average density biases of the thermospheric models during the last sunspot maximum. At altitudes of 200 to 480 km, all of the thermospheric models have a positive bias, a consequence of constructing models while assuming that the drag coefficient is independent of altitude. At 630 km the density biases of the various models diverge widely, and the uncertainty increases because drag coefficients are more uncertain there, and only one satellite was considered in that region.

Below 500 km, all the models overestimated the average atmospheric density, by amounts varying between 7% and 20%. Around 275 km, the minimum average bias was obtained with JB2008 (+8%), while around 480 km it was obtained with NRLMSISE-00 and GOST-2004 (+7%). Around 630 km, NRLMSISE-00 had a negligible bias, GOST-2004 underestimated the average atmospheric density by 11%, and the other four models continued to overestimate the average density by amounts varying between 6% and 16%. However, looking at the semi-major axis root mean square residuals, all the models considered in the study were able to provide a trajectory modeling of comparable accuracy (but with JB2006 and JB2008 consistently the best in any case), because they were able to fit the observed orbital decay with not too different residuals, with a maximum difference among the models of a factor of two. This is because even a significant constant density bias could be compensated by a properly rescaled fitted drag coefficient, still resulting in the appropriate amount of average drag force. On the other hand, if the density model is being used in efforts to validate other than drag measurements, absolute density is required.

Below 500 km, the short-term behavior of the models was also investigated by fitting the semi-major axis decay over 30-day arcs. The resulting fitted drag coefficients displayed a significant variability with all the models, probably linked to mismodeled density variations, but JB2008, followed by JB2006, returned the smallest standard deviations and the minimum semi-major axis root mean square residuals. A Fourier analysis of the results showed that the observed variability was not randomly distributed, but was the sum of some periodic components. All the models showed a term presumably associated with the perigee precession through the atmosphere, while the change of the angle between the orbit plane and the geocentric Sun vector did not play a manifest role. The similarities among most of the models also suggested that seasonal density variations, either semi-annual or annual, were possibly not fully accounted for. Moreover, the correlation of some minor terms with small multiples of the solar rotation period (e.g. 81 days) could not be ruled out. Anyway, most of the sources of the short-term variability had been evidently removed from JB2006 and JB2008, and those left resulted to have a power generally smaller than in the other models. This positive behavior was further reflected in the corresponding spectra of the semi-major axis root mean square residuals.

Acknowledgements

We are indebted to Andrey Nazarenko, who provided us with the documentation of the Russian density model, as well as with kind and useful support during the implementation of GOST-2004 in the ISTI/CNR software codes. For this we also acknowledge the support of Renzo Beltrame.

Our gratitude should be extended as well to the Naval Research Laboratory for the Fortran source of the MSISE-90 and NRLMSISE-00 models; to Space Environment Technologies for the Fortran source of the JB2006 and JB2008 models; to NOAA/NGDC for the observed solar and geomagnetic indices; to the US Space Track organization, which made available the TLEs of the satellites.

Concerning the indices of the models JB2006 and JB2008, Solar Irradiance Platform historical irradiances were provided courtesy of W. Kent Tobiska and Space Environment Technologies. These historical irradiances have been developed with partial funding from the NASA UARS, TIMED, and SOHO missions.

References

Akins, K., Healy, L., Coffey, S., Picone, M., 2003. Comparison of MSIS and Jacchia atmospheric density models for orbit determination and propagation, in: Spaceflight Mechanics 2003, Advances in the Astronautical Sciences Series, Vol. 114, Univelt Inc., San Diego, CA, USA, pp. 951-970.

Barlier, F., Berger, C., Falin, J.L., Kockarts, G., Thuillier, G., 1978. A thermospheric model based on satellite drag data. Ann. Geophys. 34, 9-24.

Bezdek, A., 2007. Lognormal distribution of the observed and modeled neutral thermospheric densities. Stud. Geophys. Geod. 51, 461-468.

Bowman, B.R., Marcos, F.A., Kendra, M.J., 2005. A method for computing accurate daily atmospheric density values from satellite drag data, in: Spaceflight Mechanics 2004, Advances in the Astronautical Sciences Series, Vol. 119, Univelt Inc., San Diego, CA, USA, pp. 1117-1134.

Bowman, B.R., Moe, K., 2006. Drag coefficient variability at 175-500 km from the orbit decay analyses of spheres, in: Astrodynamics 2005, Advances in the Astronautical Sciences Series, Vol. 123, Univelt Inc., San Diego, CA, USA, pp. 117-136.

Bowman, B.R., Tobiska, W.K., 2006. Improvements in modelling thermospheric densities using new EUV and FUV solar indices, in: Spaceflight Mechanics 2006, Advances in the Astronautical Sciences Series,Vol. 124, Univelt Inc., San Diego, CA, USA, pp. 2183-2202.

Bowman, B.R., Marcos, F.A., Moe, K., Moe, M.M., 2008a. Determination of drag coefficient values for CHAMP and GRACE satellites using orbit drag analysis, in: Astrodynamics 2007, Advances in the Astronautical Sciences Series, Vol. 129, Univelt Inc., San Diego, CA, USA, pp. 147-166.

Bowman, B.R., Tobiska, W.K., Marcos, F.A., Vallares, C., 2008b. The JB2006 empirical thermospheric density model. J. Atmos. Sol.-Terr. Phy. 70, 774-793.

Bowman, B.R., Tobiska, W.K., Marcos, F.A., Huang, C.Y., Lin, C.S., Burke, W.J., 2008c. A new empirical thermospheric density model JB2008 using new solar and geomagnetic indices. Paper AIAA 2008-6438, AIAA/AAS Astrodynamics Specialist Conference, Honolulu, Hawaii, USA, 18-21 August 2008.

Bruinsma, S.L., Thuillier, G., Barlier, F., 2003. The DTM-2000 empirical thermosphere model with new data assimilation and constraints at lower boundary: accuracy and properties. J. Atmos. Sol.-Terr. Phy. 65, 1053-1070.

Bruinsma, S.L., Tamagnan, D., Biancale, L., 2004. Atmospheric densities derived from CHAMP/STAR accelerometer observations. Planet. Space Sci. 52, 297-312.

Bruinsma, S.L., Forbes, J.M., 2007. Storm-time equatorial density enhancements observed by CHAMP and GRACE. J. Spacecraft Rockets 44 (6), 1154-1159.

Cappellari, J.O., Velez, C.E., Fuchs, A.J. (Eds.), 1976. Mathematical theory of the Goddard Trajectory Determination System. NASA/GSFC Report, GSFC X-582-76-77, Greenbelt, MD, USA, pp. 4-33–4-53.

Cefola, P.J., Nazarenko, A.I., Proulx, R.J., Yurasov, V., 2000. Neutral atmosphere density monitoring based on space surveillance system orbital data, in: Astrodynamics 1999, Advances in the Astronautical Sciences Series, Vol. 103, Univelt Inc., San Diego, CA, USA, pp. 1257-1292.

Chao, C.C., Gunning, G.R., Moe, K., Chastain, S.H., Settecerri, T.J., 1997. An evaluation of Jacchia 71 and MSIS90 atmosphere models with NASA ODERACS decay data. J. Astronaut. Sci. 45, 131-141.

Cook, G. E., 1965. Satellite drag coefficients. Planet. Space Sci. 13, 929-946.

Cook, G. E., 1966. Drag coefficients of spherical satellites. Ann. Geophys. 22, 53-64.

Doornbos, E., Klinkrad, H., Visser, P., 2005. Atmospheric density calibration using satellite drag Observations. Adv. Space Res. 36, 515-521.

Dubin, M., Hull, A.R., Champion, K.S.W., et al., 1976. US standard atmosphere 1976. NASA, NOAA and USAF, Washington, D.C., USA.

Emmert, J.T., Meier, R.R., Picone, J.M., Lean, J.L., Christensen, J.B., 2006. Thermospheric density 2002-2004: TIMED-GUVI dayside limb observations and satellite drag. J. Geophys. Res. 111, A10516, doi:10.1029/2005JA011495.

Emmert, J.T., Lean, J.L., Picone,, J.M., 2010. Record-low thermospheric density during the 2008 solar minimum. Geophys. Res. Lett. 37, L12102, 5pp, doi:10.1029/2010GL043671.

Fuller-Rowell, T.J., Rees, D., 1980. A three-dimensional, time-dependent, global model of the thermosphere. J. Atmos. Sci. 37, 2545-2567.

Fuller-Rowell, T., Codrescu, M., Moffett, R., Quegan, S., 1994. Response of the thermosphere and ionosphere to geomagnetic storms. J. Geophys. Res. 99(A3), 3893-3914.

Harris, I., Priester, W., 1965. The upper atmosphere in the range from 120 to 800 km. Reprinted in COSPAR International Reference Atmosphere. North-Holland Publ. Co., Amsterdam, The Netherlands.

Heath, B.M., Schlesinger, D.F., 1986. The Mg 280-nm douplet as a monitor of changes in solar ultraviolet irradiance. J. Geophys. Res. 91, 8672-8682.

Hedin, A.E., 1987. MSIS-86 thermospheric model. J. Geophys. Res. 92, 4649-4662.

Hedin, A.E., 1991. Extension of the MSIS thermosphere model into the middle and lower atmosphere. J. Geophys. Res. 96, 1159-1172.

Hongbo, W., Changyin, Z., 2009. Effects of various solar indices on accuracy of Earth's thermospheric neutral density models. Sci. China Ser. G: Physics, Mechanics and Astronomy 52 (7), 1120-1128.

Hoots, F.R., Roehrich, R.L., 1980. Models for propagation of NORAD elements sets. Spacetrack Report No. 3, Project Spacetrack, Aerospace Defense Command, United States Air Force, Colorado Springs, CO, USA.

Izakov, M.N., 1965. Some problems of investigating the structure of the upper atmosphere and constructing its models, in: Muller, P. (Ed.), Space Research V, North-Holland Publ. Co., Amsterdam, The Netherlands, pp. 1191-1213.

Jacchia, L.G., 1964. Static diffusion models of the upper atmosphere. Smithsonian Astrophysical Observatory, Spec. Rep. No. 170, Washington, D.C., USA.

Justus, C.G., Duvall, A., Johnson, D.L., 2004. Earth global reference atmosphere model (GRAM-99) and trace constituents. Adv. Space Res. 34 (8), 1731-1735.

King-Hele, D., 1987. Satellite Orbits in an Atmosphere. Theory and Applications. Blackie, Glasgow and London, United Kingdom, p. 198.

Koppenwallner, G., 2011. Satellite aerodynamics and determination of thermospheric density and wind, in: 27th International Symposium on Rarefied Gas Dynamics, 2010. AIP Conf. Proc. 1333, pp. 1307-1312, doi: 10.1063/1.3562824.

Kwok, J.H., 1987. The Artificial Satellite Analysis Program (ASAP), Version 2.0. JPL NPO-17522, Jet Propulsion Laboratory (JPL), Pasadena, CA, USA.

Lemoine, F.G., Kenyon, S.C., Factor, J.K., et al., 1998. The development of the joint NASA GSFC and NIMA geopotential model EGM96. NASA/TP-1998-206861. NASA Goddard Space Flight Center, Greenbelt, MD, USA.

Marcos, F.A., Wise, J.O., Kendra, M.J., Bass, J.N., Larson, D.R., Liu, J.J., 2000. Satellite drag accuracy improvements from neutral density model calibration, in: Astrodynamics 1999. Part II, Advances in the Astronautical Sciences Series, Vol. 103, Univelt Inc., San Diego, CA, USA, pp. 1227-1240.

Marcos, F.A., 2006a. New measurements of thermospheric neutral density: A review. Paper AAS 05-251, in: Astrodynamics 2005, Advances in the Astronautical Sciences Series, Vol. 123, Univelt Inc., San Diego, CA, USA, pp. 3-14.

Marcos, F.A., 2006b. New satellite drag modeling capabilities, Paper AIAA 2006-470, 44th AIAA Aerospace Sciences meeting and Exhibit, Reno, Nevada, USA, 9-12 January 2006.

McLaughlin, C.A., Hiatt, A., Lechtenberg, T., 2011. Precision orbit derived total density. J. Spacecraft Rockets 48 (1), 166-174.

Moe, M.M., Wallace, S.D., Moe, K., 1995. Recommended drag coefficients for aeronomic satellites, in: The Upper Mesosphere and Lower Thermosphere: A Review of Experiment and Theory, Geophysical Monograph 87, 349-356.

Moe, K., Moe, M.M., Wallace, S.D., 1998. Improved satellite drag coefficient calculations from orbital measurements of energy accommodation. J. Spacecraft Rockets 35, 266-272.

Moe, K., Moe, M.M., Rice, C.J., 2004. Simultaneous analysis of multi-instrument satellite measurements of atmospheric density. J. Spacecraft rockets 41, 849-853.

Moe, K., Moe, M.M., 2005. Gas-surface interactions and satellite drag coefficients. Planet. Space Sci. 53, 793-801.

Moe, K., 2006. Progress in predicting the decay of satellite and debris orbits. Third Annual AIAA Southern California Aerospace System and Technology Conference, 3 May 2006.

Moe, K., Moe, M.M., 2008. The high-latitude thermosphere mass density anomaly: a historical review and a semi-empirical model. J. Atmos. Sol.-Terr. Phy.70, 794-802.

Moe, K, Moe. M.M., 2011a. Gas-surface interactions in low-Earth orbit, in: 27th International Symposium on Rarefied Gas Dynamics, 2010. AIP Conf. Proc. 1333, pp. 1313-1318, doi: 10.1063/1.3562825.

Moe, K., Moe, M.M., 2011b. Operational models and drag-derived density trends in the thermosphere. Space Weather 9, S00E10, doi:10.1029/2010SW000650.

Nazarenko, A., 1999. Atmospheric density tracking studies. Report prepared by the Scientific Industrial Firm NUCOL for the Charles Stark Draper Laboratory, CSDL-C-6505.

Nazarenko, A., Yurasov, V., 2003. Atmospheric density correction using real orbital data, in: Proceedings of the 17th International Symposium on Space Flight Dynamics, Moscow, Russia, 16-20 June 2003, Published by Keldysh Institute of Applied Mathematics, Space Informatics Analytical Systems (KIA Systems), Moscow, Russia, pp. 327-342.

Owens, J.K., 2002. NASA Marshall Engineering Thermosphere Model – Version 2.0. Technical Memorandum NASA / TM--2002-211786, NASA Marshall Space Flight Center (MSFC), Alabama, USA.

Paxton, L.J., et al., 1992. Special sensor UV spectrographic imager (SSUSI): An instrument description. Instrum. Planet Terr. Atmos. Remote Sens., 1745, 2-16.

Pardini, C., Anselmo, L., 1994. SATRAP: Satellite reentry analysis program. Internal Report C94-17, CNUCE Institute, Consiglio Nazionale delle Ricerche (CNR), Pisa, Italy.

Pardini, C., Anselmo, L., 2001. Comparison and accuracy assessment of semi-empirical atmosphere models through the orbital decay of spherical satellites. J. Astronaut. Sci. 49 (2), pp. 255-268.

Pardini, C., Anselmo, L., 2003. Performance evaluation of atmospheric density models for satellite reentry predictions with high solar activity levels. T. Jpn. Soc. Aeronaut. S. (JSASS 46 (151), pp. 42-46.

Pardini, C., Tobiska, W.K., Anselmo , L., 2006. Analysis of the orbital decay of spherical satellites using different solar flux proxies and atmospheric density models. Adv. Space Res. 37 (2), 392-400.

Pardini, C., Anselmo, L., 2008a. Impact of the time span selected to calibrate the ballistic parameter on spacecraft re-entry predictions. Adv. Space Res. 41 (7), 1100-1114.

Pardini, C., Anselmo, L., 2008b. Long-term evolution of geosynchronous orbital debris with high area-to-mass ratios. T. Jpn. Soc. Aeronaut. S. 51 (171), 22-27.

Pardini, C., Anselmo, L., Moe, K., Moe, M.M., 2010. Drag and energy accommodation coefficients during sunspot maximum. Adv. Space Res. 45, 638-650.

Picone, J.M., Hedin, A.E., Drob, D.P., Lean, J., 2002. NRLMSISE-00 empirical model: comparisons to data and standard models, in: Astrodynamics 2001, Advances in the Astronautical Sciences Series, Vol. 109, Univelt Inc., San Diego, CA, USA, pp. 1385-1398.

Picone, J.M., Hedin, A.E., Drob, D.P., Aikan, A.C., 2002. NRLMSISE-00 empirical model of the atmosphere: statistical comparisons and scientific issues. J. Geophys. Res. 107 (A12), 1468, doi:10.1029/2002JA009430.

Pilinski, M., Argrow, B., Palo, S., 2010. Semi-empirical model for satellite energy-accommodation coefficients. J. Spacecraft Rockets 47 (6), 951-956.

Qian, L., Solomon, S. C., Kane, T. J., 2009. Seasonal variation of thermospheric density and composition. J. Geophys. Res. 114, A01312, doi:10.1029/2008JA013643.

Regan, F.J., Anandakrishnan, S.M., 1993. Dynamics of atmospheric re-entry. AIAA Education Series, American Institute of Aeronautics and Astronautics, Washington, D.C., USA, pp. 313-317.

Sehnal, L., 1988. Thermospheric total density model TD. Bull. Astron. Inst. Czechosl. 39, 120-127.

Sehnal, L., Pospisilova, L., 1988. Thermospheric model TD 88. Preprint No. 67, Astronomical Institute, Czechoslovak Academy of Sciences, Czechoslovakia.

Sentman, L.H., 1961. Free molecule flow theory and its application to the determination of aerodynamic forces. Lockheed Missile and Space Co., KMSC-448514, AD 265-409.

Solomon, S.C. Woods, T.N., Didkovsky, L.V., Emmert, J.T., Qian, L., 2010. Anomalously low solar extreme-ultaviolet irradiance and thermospheric density during solar minimum. Geophys. Res. Lett. 37, L16103, doi:10.1029/2010GL044468.

Storz, M.F., Bowman, B.R., Branson, J.I., 2002. High Accuracy Satellite Drag Model (HASDM), Paper AIAA 2002-4886, AIAA/AAS Astrodynamics Specialist Conference, Monterey, CA, USA, 5-8 August 2002.

Tobiska, W.K., Bouwer, S.D., Bowman, B.R., 2008. The development of new solar indices for use in thermospheric density modeling. J. Atmos. Sol.-Terr. Phy. 70, 803-819.

Vallado, D.A., 2007. A preliminary analysis of state vector prediction accuracy, Paper AAS 07-358, AAS/AIAA Astrodynamics Specialist Conference, Mackinac Island, Michigan, USA, 19-23 August 2007.

Vallado, D.A., Crawford, P., 2008. SGP4 orbit determination, Paper AIAA 2008-6770, AIAA/AAS Astrodynamics Specialist Conference and Exhibit, Honolulu, Hawaii, USA, 18-21 August 2008.

Vallado, D.A., Finkleman, D., 2008. A critical assessment of satellite drag and atmospheric density modeling, Paper AIAA 2008-6642, AIAA/AAS Astrodynamics Specialist Conference and Exhibit, Honolulu, Hawaii, USA, 18-21 August 2008.

Volkov, I.I., Yastrebov, V.V., 1990. The improvement of the atmospheric density model using COSMOS satellite orbital evolution, Nabludeniya Isk. Sputn., Astronomical Council of the USSR Acad. No. 86.

Volkov, I.I., 2004. Earth's upper atmosphere density model for ballistic support of the flight of artificial Earth satellites GOST R 25645.166-2004. Publishing House of the Standards, Moscow.

Volkov, I.I., Suevalov, V.V., 2005. Estimation of long-term density variations in the upper atmosphere of the Earth at minimum of solar activity from evolution of the orbital parameters of the Earth's artificial satellites. Sol. Syst. Res. 39 (2), 157-162.

Volkov, I.I., Semenov, A.I., Suevalov, V.V., 2008. Analysis of thermospheric density variations neglected in modern atmospheric models using accelerometer data. Sol. Syst. Res. 42 (1), 51-62.

Wolverton, R.W. (Ed.), 1963. Flight Performance Handbook for Orbital Operations. Wiley, New York (USA) and London (UK), pp. 2-336 – 2-339.

Yurasov, V.S., Nazarenko, A.I., Cefola, P.J., Alfriend, K.T., 2004. Results and issues of atmospheric density corrections, Paper AAS 04.305, Proceedings of the 14th AAS/AIAA Space Flight Mechanics Meeting, Maui, Hawaii, USA, 8-12 February 2004.

Yurasov, V.S., Nazarenko, A. I., Alfriend, K.T., Cefola, P.J., 2006. Direct density correction method: review and results, 57th International Astronautical Congress, Paper IAC-06-C1.5.2, Valencia, Spain, 2-6 October 2006.

Figure captions

Figure 1. Drag coefficients in low-Earth orbit using parameters measured in orbit during sunspot minimum.

Figure 2. Daily and 81-day centered average solar radio flux at 10.7 cm during the maximum of solar cycle 23.

Figure 3. Daily geomagnetic planetary index A_p during the maximum of solar cycle 23.

Figure 4. 81-day centered average of the $F_{10.7}$, $S_{10.7}$, $M_{10.7}$, and $Y_{10.7}$ solar irradiance indices during the maximum of solar cycle 23.

Figure 5. Thirty-day arc fitted drag coefficients (C_{DF}) and semi-major axis root mean square residuals (R) for Cosmos 2265, Cosmos 2332 and SNOE, using JR-71 as density model.

Figure 6. Thirty-day arc fitted drag coefficients (C_{DF}) and semi-major axis root mean square residuals (R) for Cosmos 2265, Cosmos 2332 and SNOE, using MSISE-90 as density model.

Figure 7. Thirty-day arc fitted drag coefficients (C_{DF}) and semi-major axis root mean square residuals (R) for Cosmos 2265, Cosmos 2332 and SNOE, using NRLMSISE-00 as density model.

Figure 8. Thirty-day arc fitted drag coefficients (C_{DF}) and semi-major axis root mean square residuals (R) for Cosmos 2265, Cosmos 2332 and SNOE, using GOST-2004 as density model.

Figure 9. Thirty-day arc fitted drag coefficients (C_{DF}) and semi-major axis root mean square residuals (R) for Cosmos 2265, Cosmos 2332 and SNOE, using JB2006 as density model.

Figure 10. Thirty-day arc fitted drag coefficients (C_{DF}) and semi-major axis root mean square residuals (R) for Cosmos 2265, Cosmos 2332 and SNOE, using JB2008 as density model.

Figure 11. Fourier analysis of the 30-day arc fitted drag coefficients (C_{DF}) and semi-major axis root mean square residuals (R) obtained with the JR-71 density model.

Figure 12. Fourier analysis of the 30-day arc fitted drag coefficients (C_{DF}) and semi-major axis root mean square residuals (R) obtained with the MSISE-90 density model.

Figure 13. Fourier analysis of the 30-day arc fitted drag coefficients (C_{DF}) and semi-major axis root mean square residuals (R) obtained with the NRLMSISE-00 density model.

Figure 14. Fourier analysis of the 30-day arc fitted drag coefficients (C_{DF}) and semi-major axis root mean square residuals (R) obtained with the GOST-2004 density model.

Figure 15. Fourier analysis of the 30-day arc fitted drag coefficients (C_{DF}) and semi-major axis root mean square residuals (R) obtained with the JB2006 density model.

Figure 16. Fourier analysis of the 30-day arc fitted drag coefficients (C_{DF}) and semi-major axis root mean square residuals (R) obtained with the JB2008 density model.

Table 1

Satellites used in the study

Satellite Name	Catalog Number	Area [m^2]	Mass [kg]	Mean orbital elements at the beginning of the time span			Time span over which the orbital decay was analyzed
				Inclination [deg]	Perigee Altitude [km]	Apogee Altitude [km]	
Cylinder-like body with a hexagonal cross section							
SNOE	25233	0.8377	115.5	97.7	515	570	2-Oct-99 30-Dec-02
Spinning box with solar panels and a long rod for gravity-gradient stabilization							
Clementine	25968	0.568	50	98.1	643	663	4-Dec-99 30-Dec-02
TAIFUN YUGS spheres							
Cosmos 2265	22875	3.142	750	82.8	280	1279	2-Oct-99 30-Dec-02
Cosmos 2332	23853	3.142	750	82.9	286	1383	1-Oct-99 30-Dec-02

Table 2

Fitted drag coefficients (C_{DF}) and root mean squares residuals on semi-major axis (R) using different thermospheric density models during the maximum of solar cycle 23

Density Model	JR-71	MSISE-90	NRLMSISE-00	GOST-2004	JB2006	JB2008
Cosmos 2265						
C_{DF}	1.90	1.93	1.96	1.96	1.90	1.98
R	1555 m	2450 m	1939 m	2273 m	990 m	1415 m
Cosmos 2332						
C_{DF}	1.91	1.93	1.97	1.97	1.91	1.99
R	1398 m	2164 m	1727 m	1996 m	1035 m	1020 m
SNOE						
C_{DF}	2.02	2.24	2.34	2.33	2.13	2.29
R	917 m	1187 m	1246 m	894 m	654 m	626 m
Clementine						
C_{DF}	2.21	2.48	2.63	2.93	2.24	2.41
R	493 m	476 m	409 m	367 m	259 m	224 m

Table 3

Estimated physical drag coefficients of the satellites

Average Perigee Altitude [km]	Satellite	Physical Drag Coefficient C_{DP}
272	Cosmos 2265	2.15
280	Cosmos 2332	2.16
476	SNOE	2.51
625	Clementine	2.64

Table 4

Average density biases of the thermospheric models at sunspot maximum

Satellite (Mean Perigee Altitude)	THERMOSPHERIC DENSITY MODEL					
	JR-71	**MSISE-90**	**NRLMSISE-00**	**GOST-2004**	**JB2006**	**JB2008**
Cosmos 2265 (272 km)	+11.6%	+10.2%	+8.8%	+8.8%	+11.6%	+7.9%
Cosmos 2332 (280 km)	+11.6%	+10.6%	+8.8%	+8.8%	+11.6%	+7.9%
SNOE (476 km)	+19.5%	+10.8%	+6.8%	+7.2%	+15.1%	+8.8%
Clementine (625 km)	+16.3%	+6.1%	~0%	−11.0%	+15.2%	+8.7%

Table 5

Thirty-day arc semi-major axis average root mean square residuals $\langle R \rangle$ and standard deviations σ_R

Density Model	JR-71	MSISE-90	NRLMSISE-00	GOST-2004	JB2006	JB2008
Cosmos 2265						
$\langle R \rangle$ [m]	102.5	100.6	100.3	145.4	81.3	83.9
σ_R [m]	50.0	41.8	45.4	75.2	30.9	28.1
Cosmos 2332						
$\langle R \rangle$ [m]	110.9	96.5	96.3	118.8	89.8	83.2
σ_R [m]	46.8	36.8	39.5	54.7	31.6	33.4
SNOE						
$\langle R \rangle$ [m]	72.0	70.2	70.3	76.2	59.5	66.1
σ_R [m]	26.4	19.7	19.4	30.5	13.1	21.2

Highlights

- Six thermospheric density models were analyzed: JR-71, MSISE-90, NRLMSISE-00, GOST-2004, JB2006 and JB2008.
- For each density model, fitted drag coefficients were obtained for a sample of satellites by analyzing their orbital decay.
- The average density biases of the thermospheric models were estimated during the maximum of solar cycle 23.
- Below 500 km, all the models overestimated the average atmospheric density by amounts varying between +7% and +20%.
- The minimum average biases were obtained with JB2008, NRLMSISE-00 and GOST-2004.

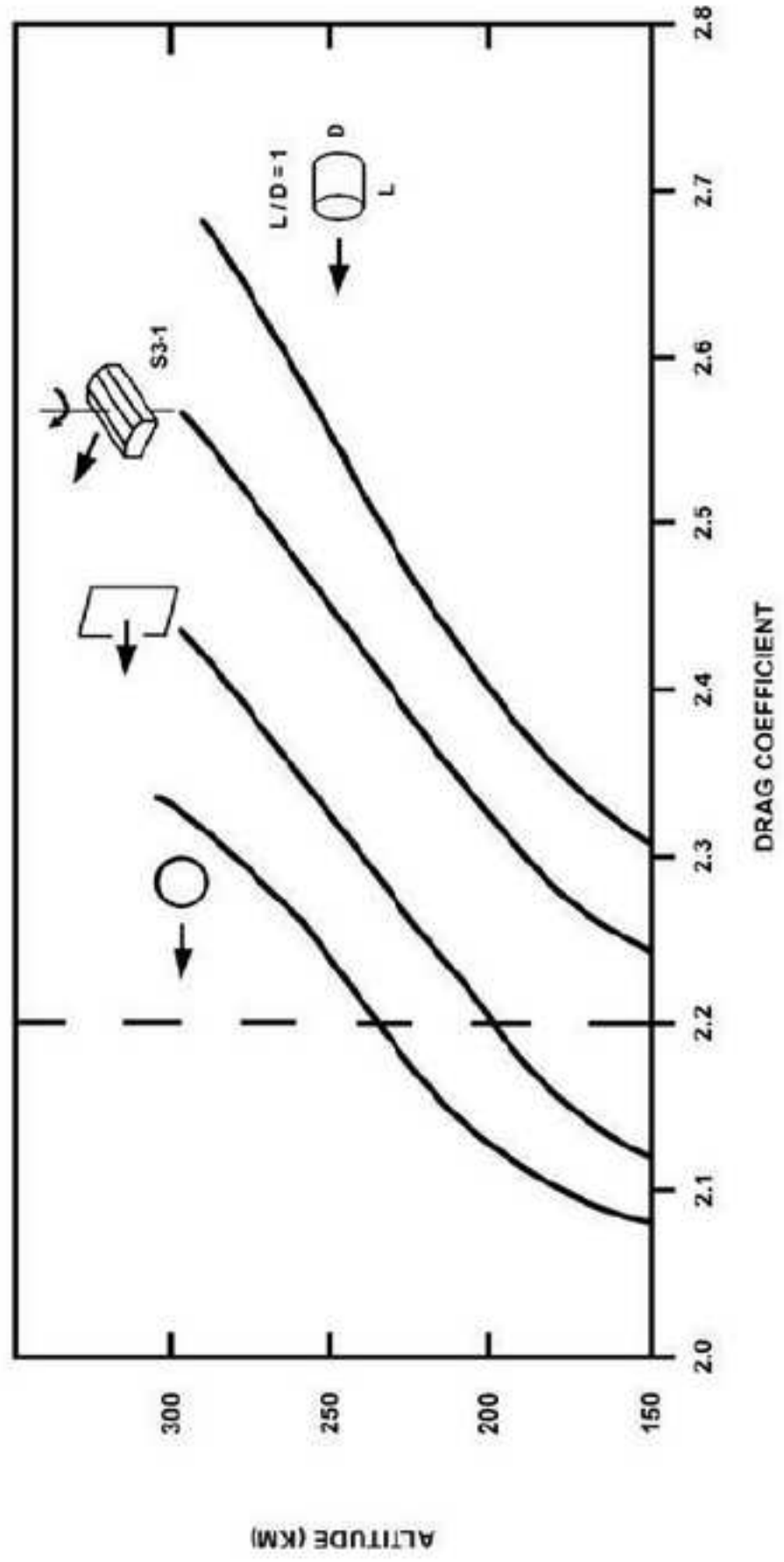
ALTITUDE (KM)
300
250
200
150
2.0
2.1
2.2
2.3
2.4
2.5
2.6
2.7
2.8
DRAG COEFFICIENT
L/D=1
D
L
S3-1

Figure-01

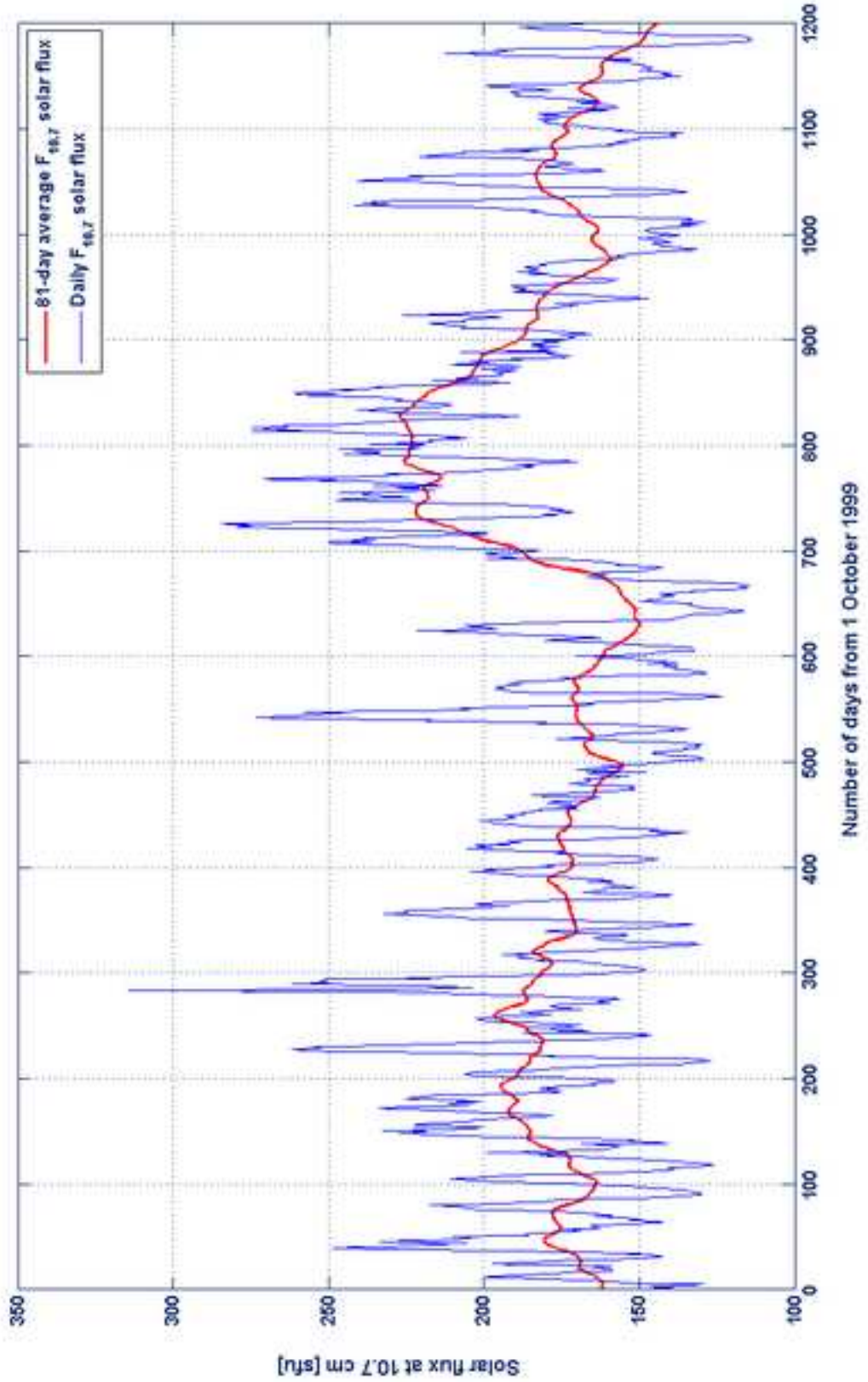
81-day average $F_{10.7}$ solar flux
Daily $F_{10.7}$ solar flux
Solar flux at 10.7 cm [sfu]
Number of days from 1 October 1999
350
300
250
200
150
100
0
100
200
300
400
500
600
700
800
900
1000
1100
1200

Figure-02

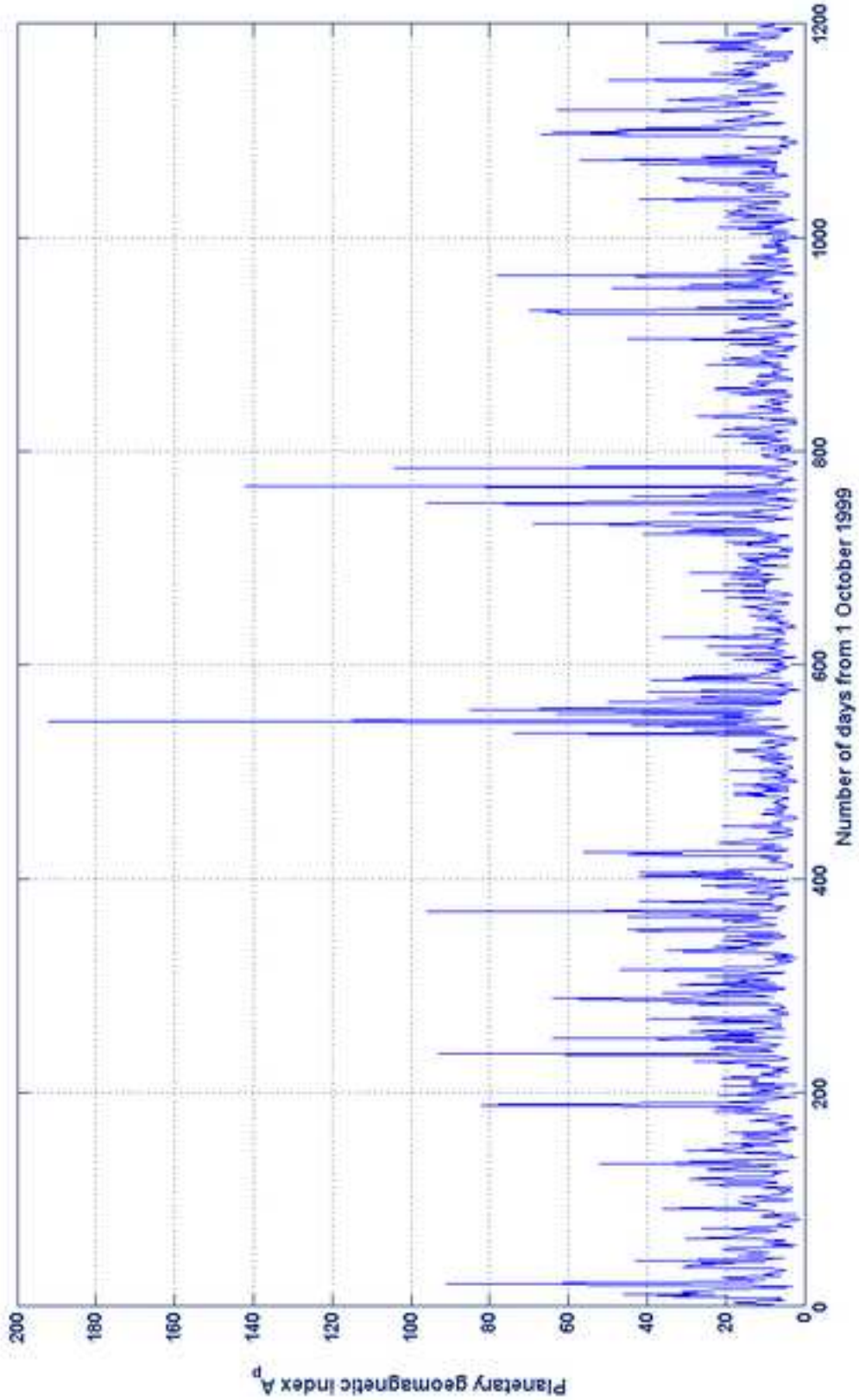
Planetary geomagnetic index A_p
0
20
40
60
80
100
120
140
160
180
200
Number of days from 1 October 1999
0
200
400
600
800
1000
1200

Figure-03

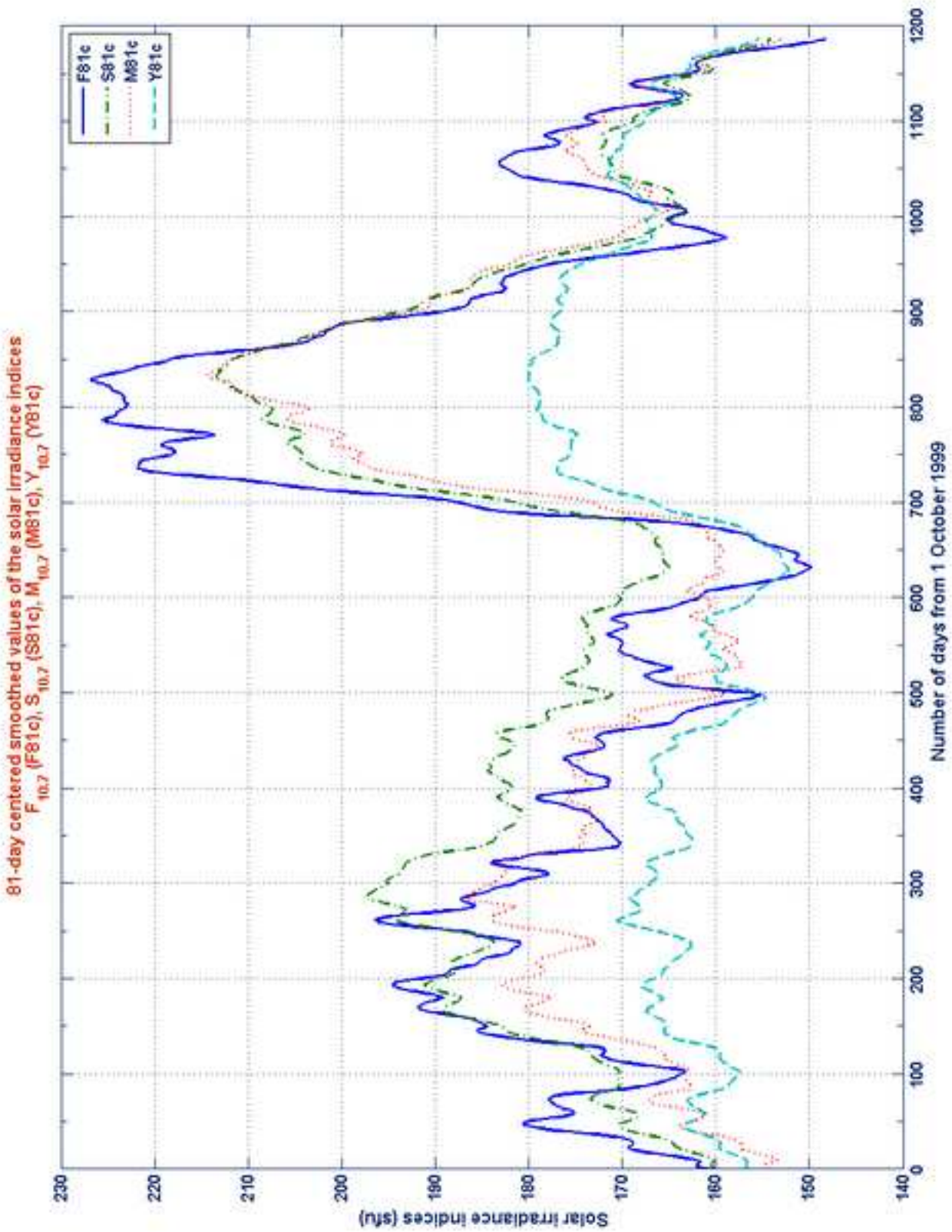
81-day centered smoothed values of the solar irradiance indices
$F_{10.7}$ (F81c), $S_{10.7}$ (S81c), $M_{10.7}$ (M81c), $Y_{10.7}$ (Y81c)
F81c
S81c
M81c
Y81c
Solar irradiance indices (sfu)
Number of days from 1 October 1999
230
220
210
200
190
180
170
160
150
140
0
100
200
300
400
500
600
700
800
900
1000
1100
1200

Figure-04

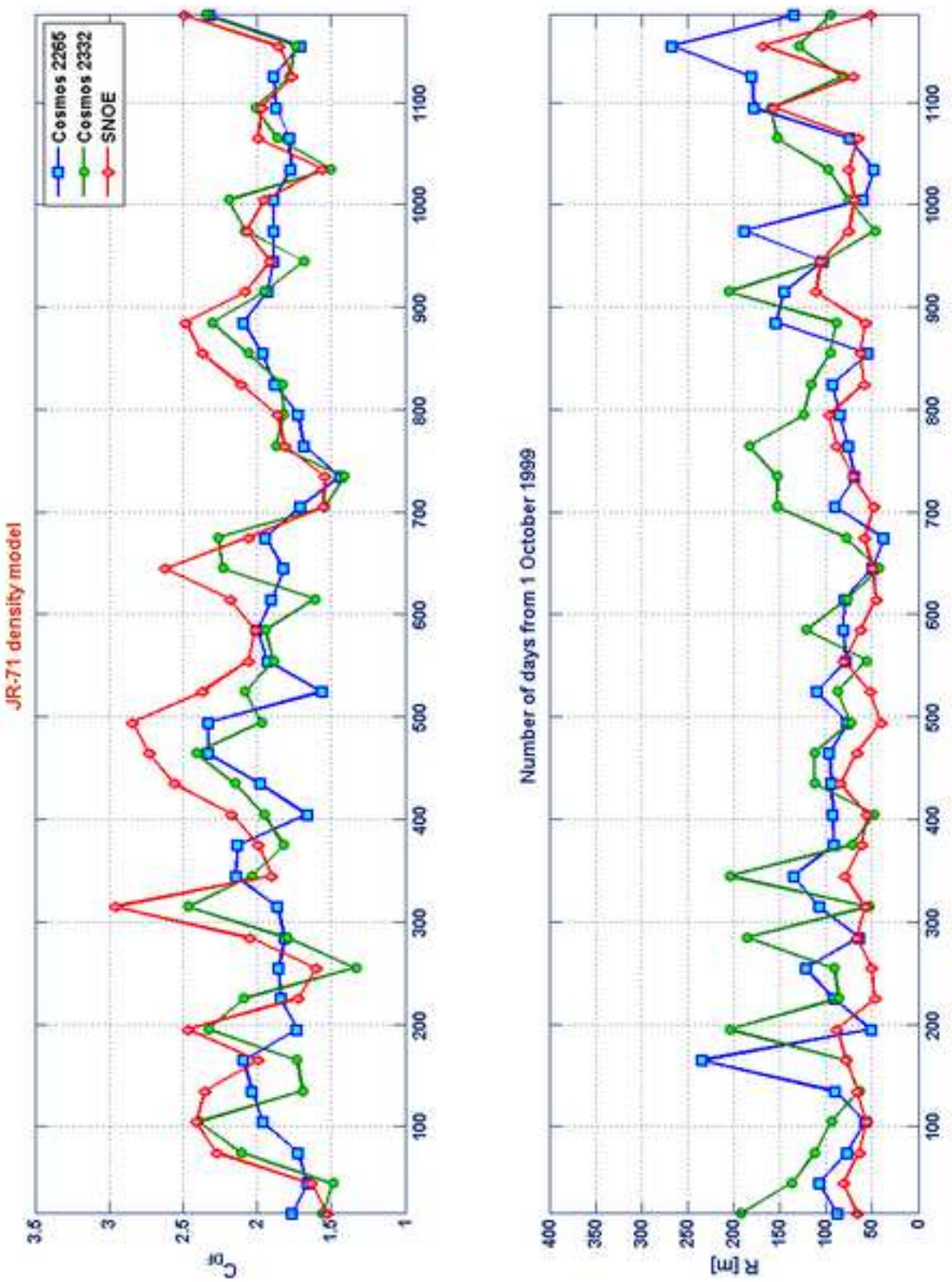
JR-71 density model
Cosmos 2265
Cosmos 2332
SNOE
C_{DF}
Number of days from 1 October 1999
R [m]

Figure-05

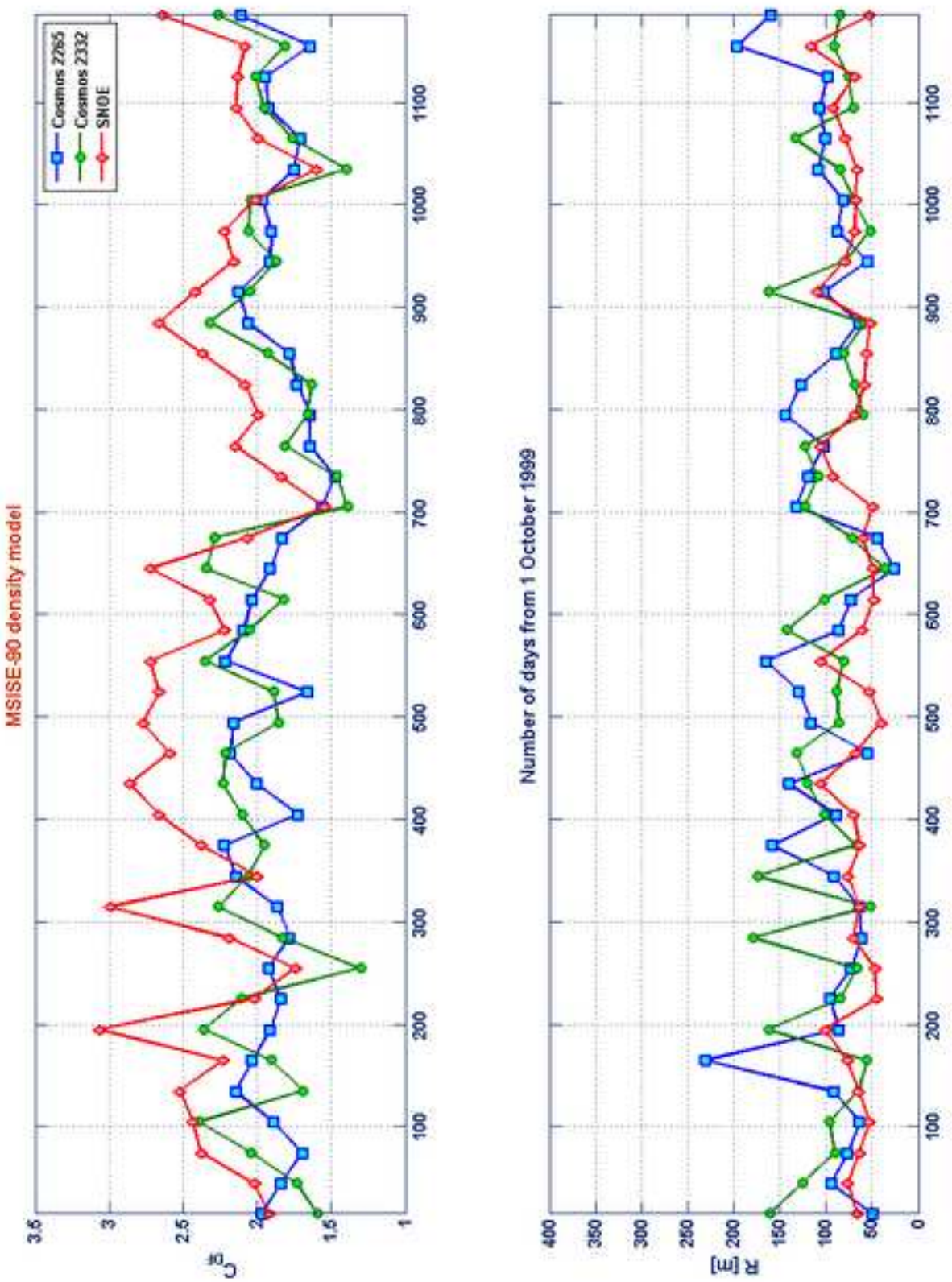
Cosmos 2265
Cosmos 2332
SNOE
MSISE-90 density model
C_{DR}
Number of days from 1 October 1999
R [m]

Figure-06

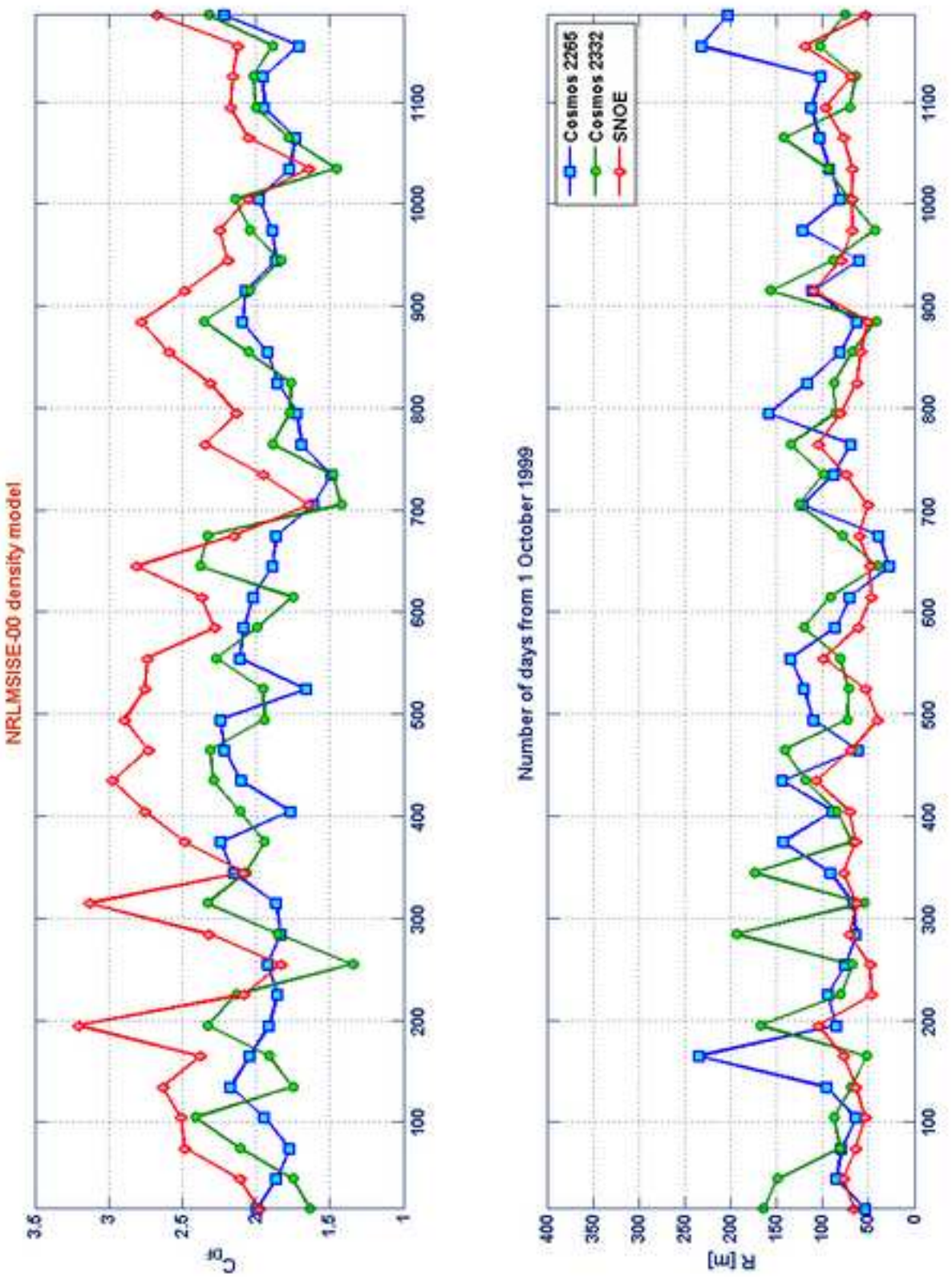
NRLMSISE-00 density model
C_{DF}
Number of days from 1 October 1999
R [m]
Cosmos 2265
Cosmos 2332
SNOE

Figure-07

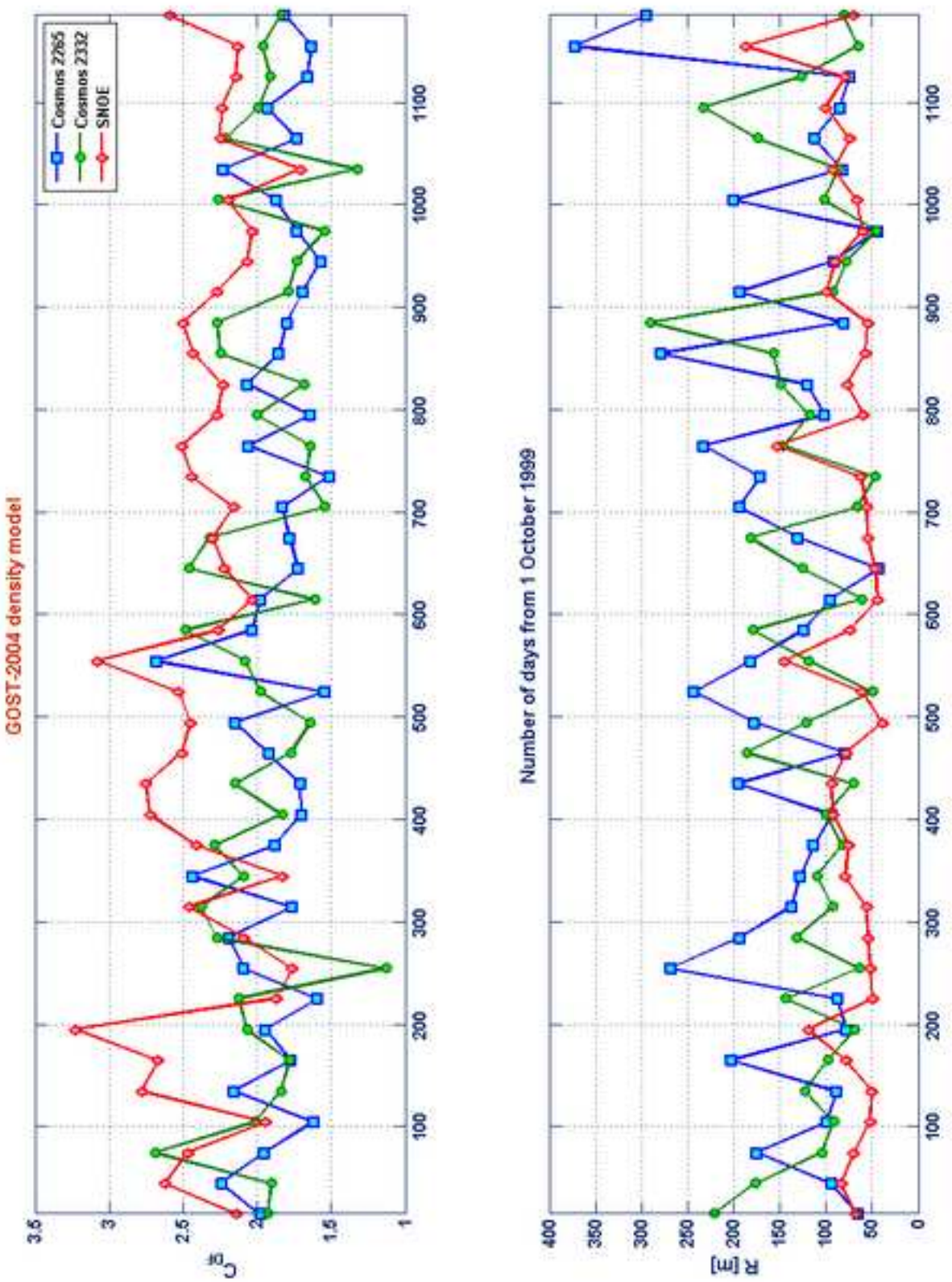
Cosmos 2265
Cosmos 2332
SNOE
GOST-2004 density model
C_{DF}
Number of days from 1 October 1999
R [m]

Figure-08

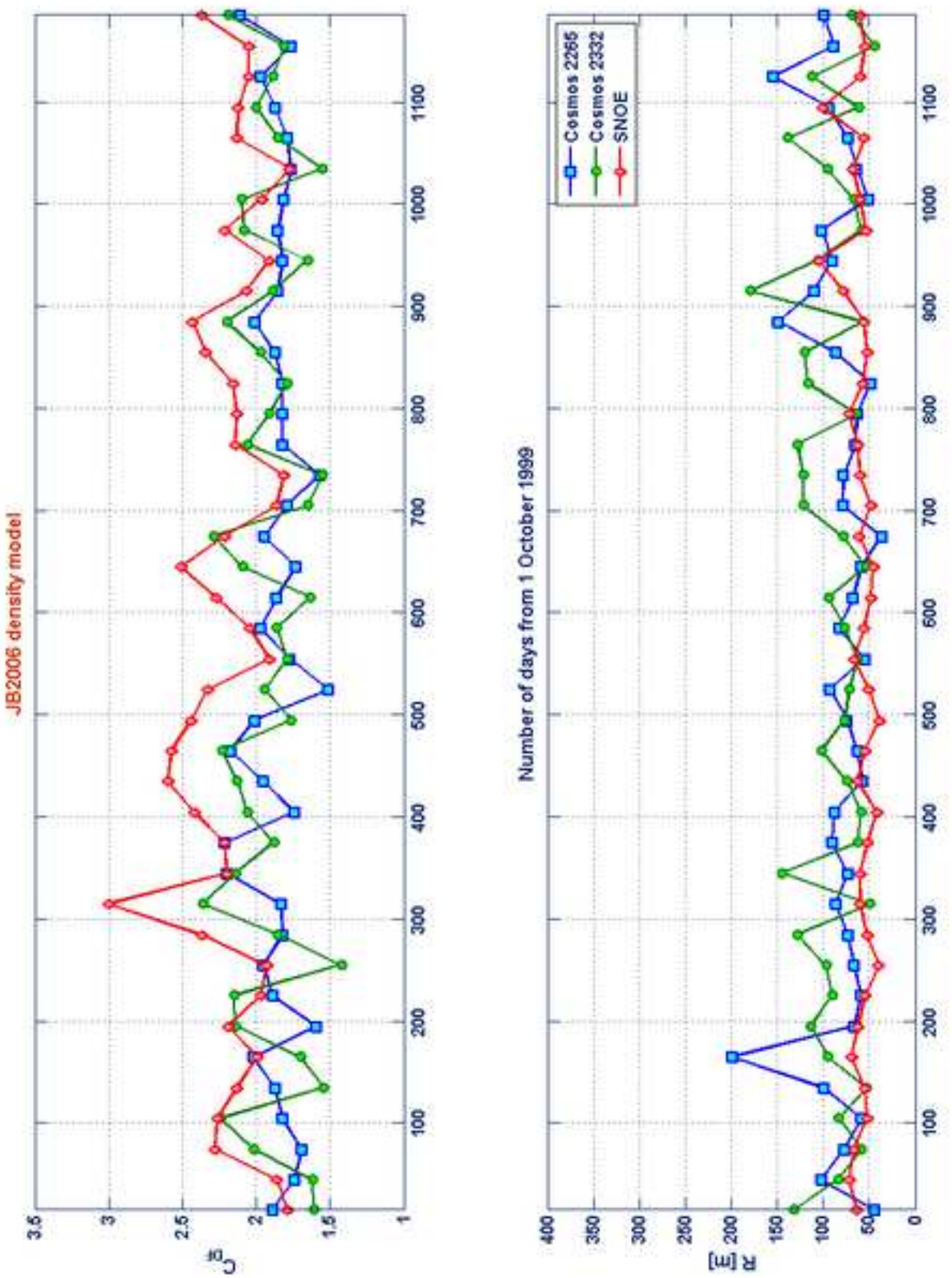
JB2006 density model
C_{DR}
Number of days from 1 October 1999
R [m]
Cosmos 2265
Cosmos 2332
SNOE

Figure-09

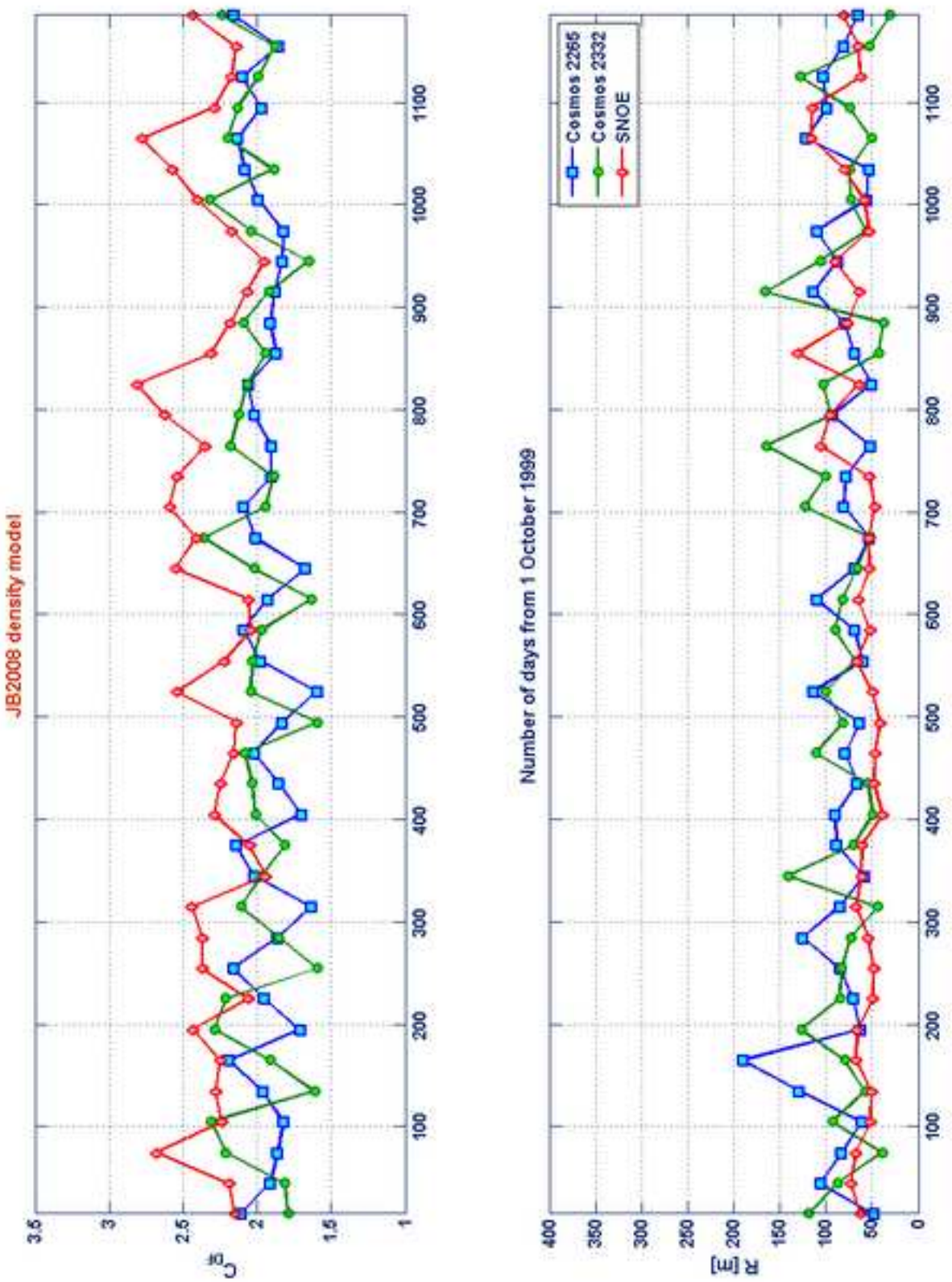
JB2008 density model
C_R
Number of days from 1 October 1999
R [m]
Cosmos 2265
Cosmos 2332
SNOE

Figure-10

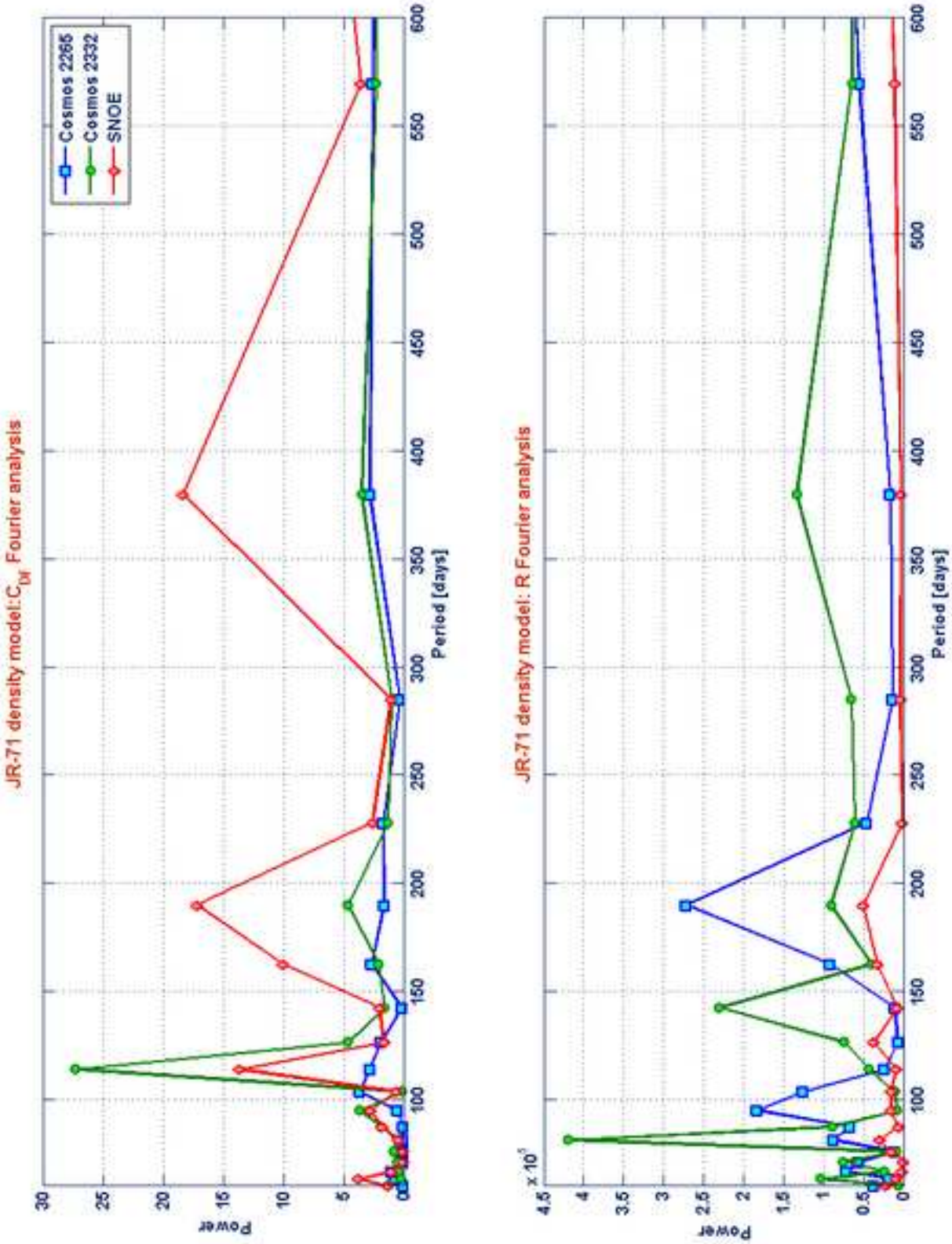

Figure-11

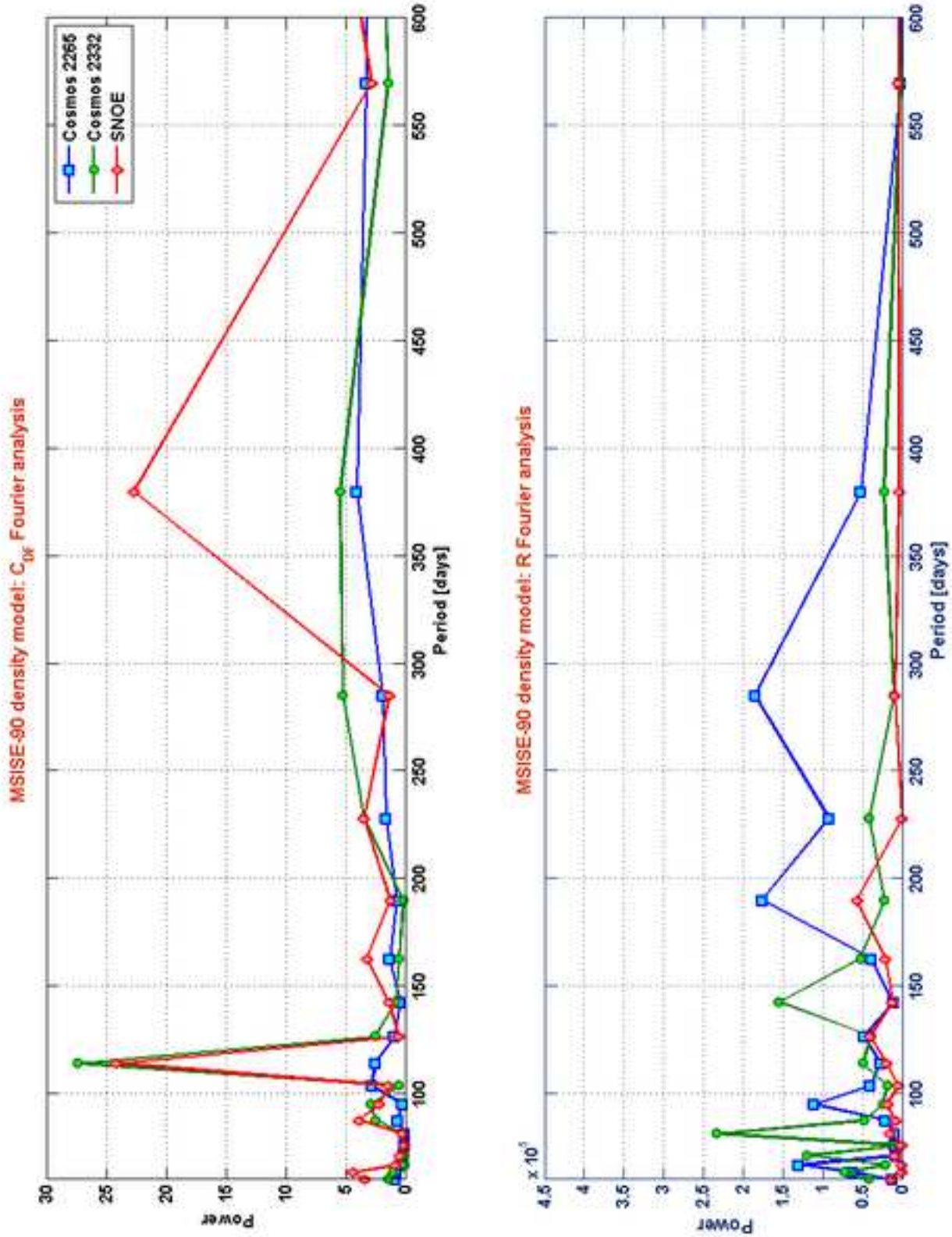
MSISE-90 density model: C_{DF} Fourier analysis
Cosmos 2265
Cosmos 2332
SNOE
Power
Period [days]
MSISE-90 density model: R Fourier analysis
x 10^-1
Power
Period [days]

Figure-12

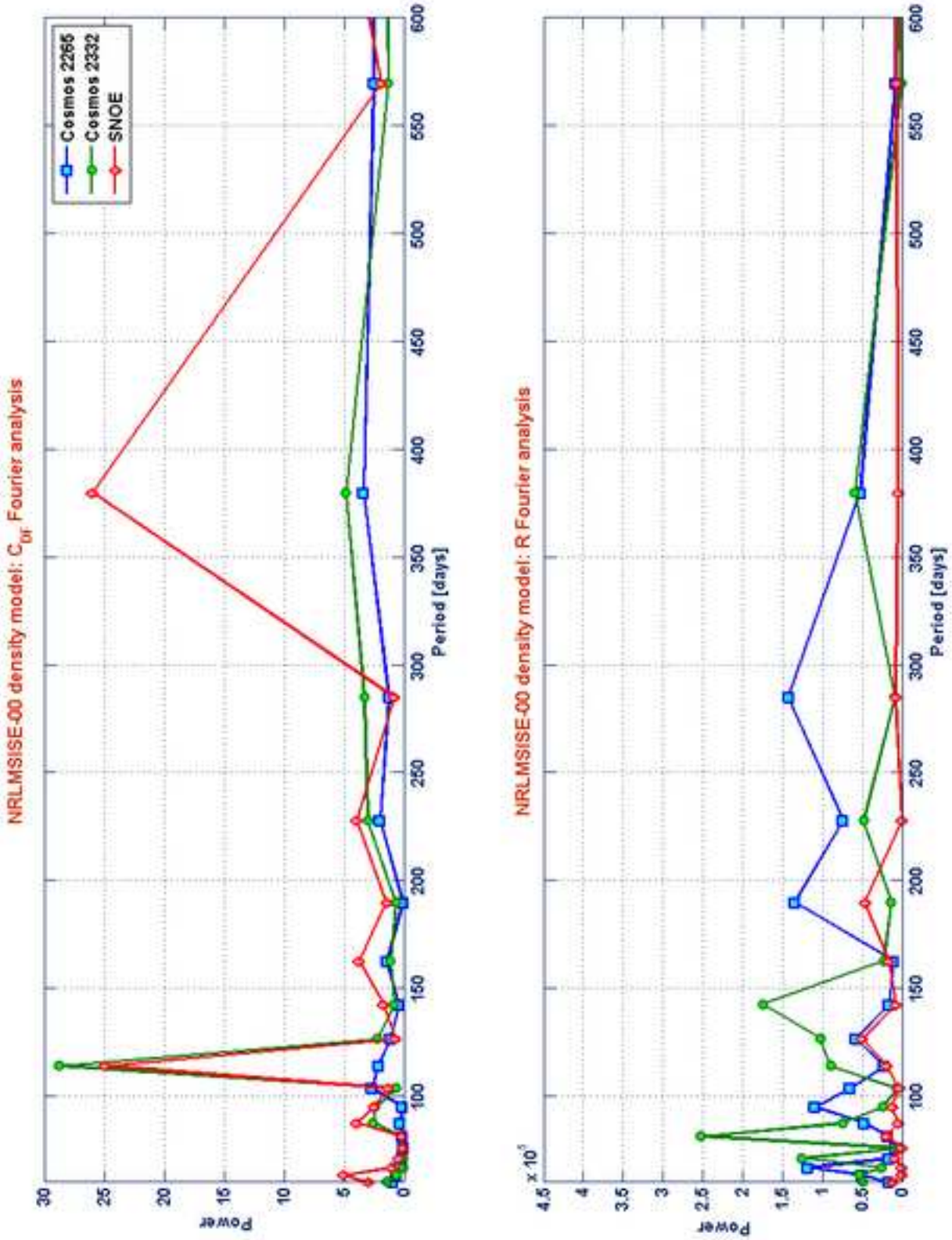
NRLMSISE-00 density model: C_{DF} Fourier analysis
Cosmos 2265
Cosmos 2332
SNOE
Power
Period [days]
NRLMSISE-00 density model: R Fourier analysis
x 10^-1
Power
Period [days]

Figure-13

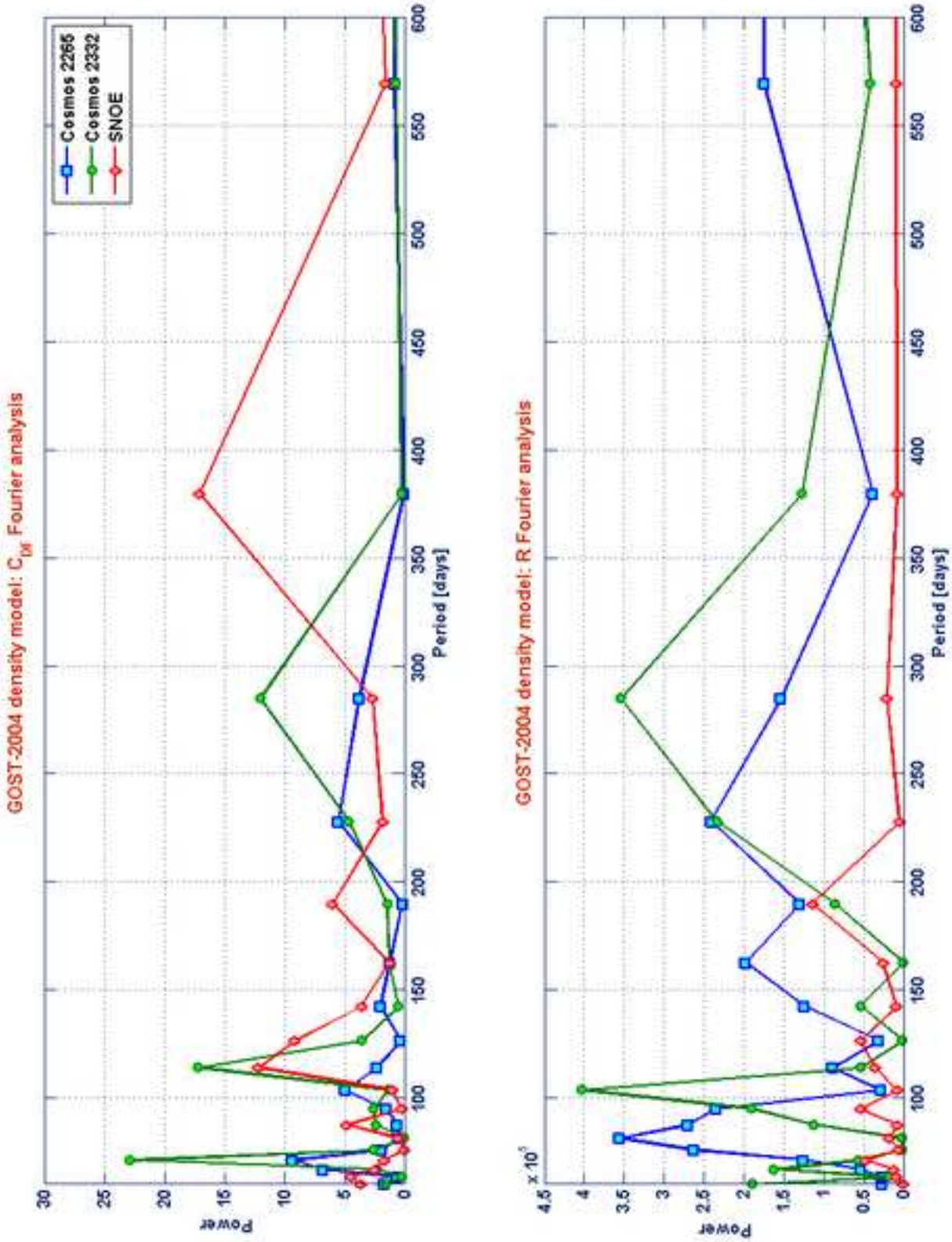
GOST-2004 density model: C_{DF} Fourier analysis
Cosmos 2265
Cosmos 2332
SNOE
Power
Period [days]
GOST-2004 density model: R Fourier analysis
x 10^-1
Power
Period [days]

Figure-14

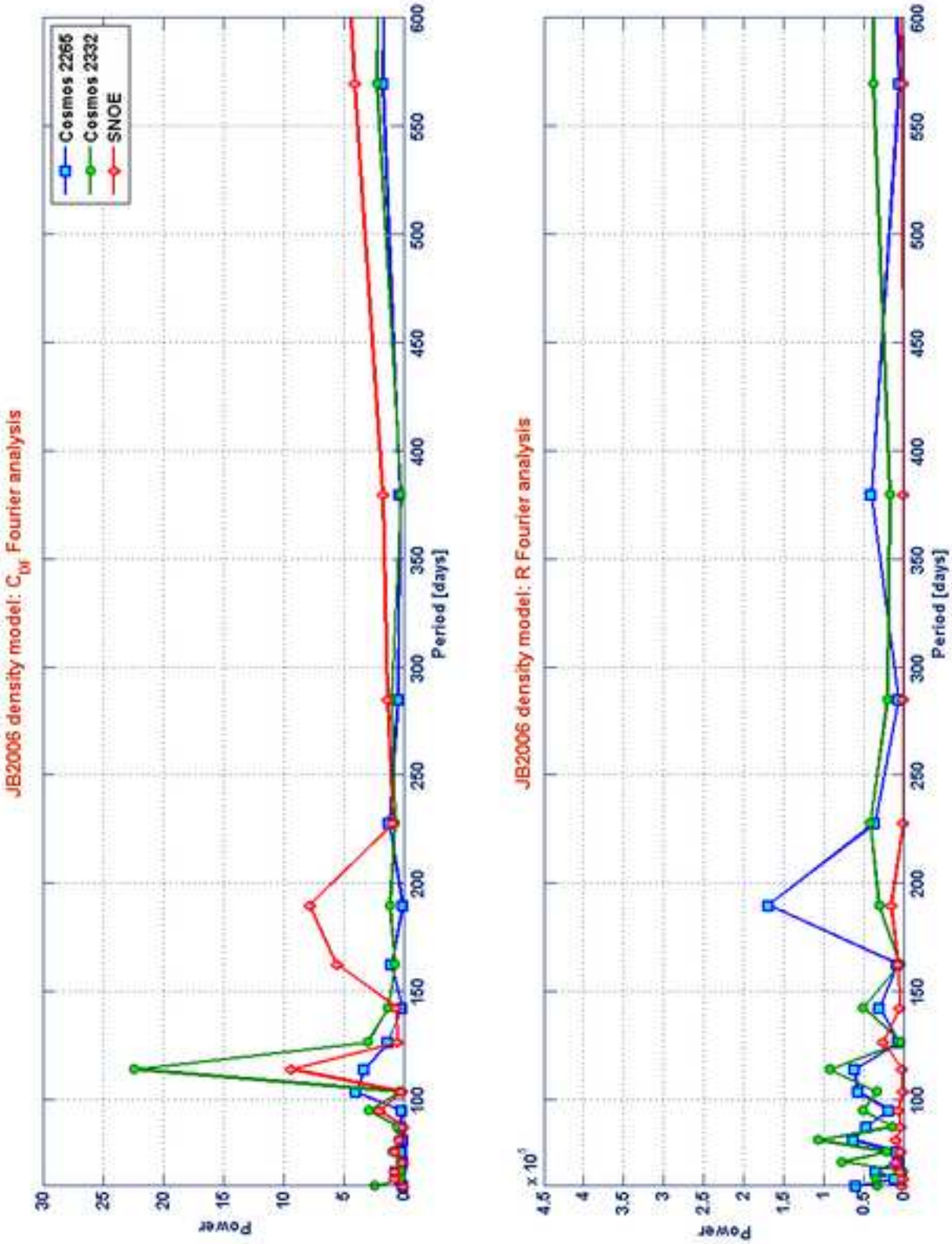
JB2006 density model: C_W Fourier analysis
Cosmos 2265
Cosmos 2332
SNOE
Power
Period [days]
JB2006 density model: R Fourier analysis
x 10^-1
Power
Period [days]

Figure-15

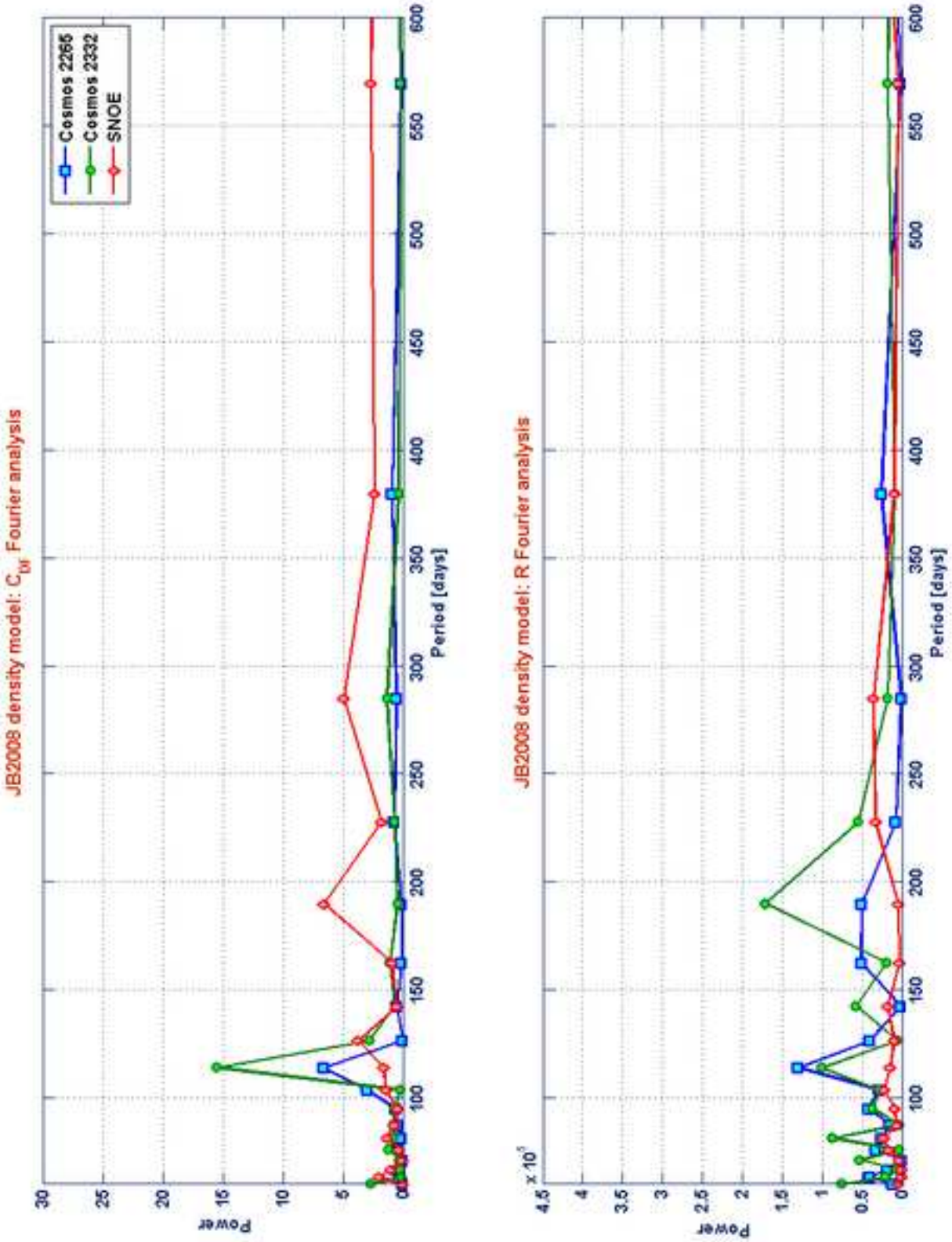
JB2008 density model: C_{bf} Fourier analysis
Cosmos 2265
Cosmos 2332
SNOE
Power
Period [days]
JB2008 density model: R Fourier analysis
x 10^-1
Power
Period [days]

Figure-16